# Global genome analysis identifies glycolipids and lipoteichoic acid alanylation as contributors to Group B streptococcal diabetic wound infection

Luke R. Joyce[1], Madeline S. Akbari[1], Dustin T. Nguyen[1], Brady L. Spencer[1,2], Jeremy Rahkola[3], Kevin S. McIver[4], Alexander R. Horswill[1,3], Kelly S. Doran[1,*], and Rebecca A. Keogh[1,*]

[1]Department of Immunology and Microbiology, University of Colorado Anschutz, Aurora, CO, USA
[2]Department of Microbiology, Immunology, and Cancer Biology, University of Viriginia School of Medicine, Virginia, USA
[3]Department of Veterans Affairs, Eastern Colorado Healthcare System, Aurora, CO, USA.
[4]Cell Biology and Molecular Genetics, Maryland Pathogen Research Institute, University of Maryland, College Park, Maryland, USA

*Correspondence: Kelly.Doran@CUAnschutz.edu, Rebecca.Keogh@ CUAnschutz.edu

## ABSTRACT

Individuals with diabetes frequently develop chronic, hyper-inflammatory, non-healing wounds, which are the leading cause of all non-traumatic amputations. Group B *Streptococcus* (GBS) is a prominent bacterium isolated from diabetic wound infections and in a murine model of diabetic wound infection, GBS stimulates an influx of neutrophils into the wound. Utilizing a transposon mutant screen, we identified 291 bacterial genes required for fitness during diabetic wound infection including enzymes involved in glycolipid biosynthesis and lipoteichoic acid (LTA) alanylation. GBS mutants lacking either LTA alanylation (Δ*dltA*) or all glycolipids (Δ*iagB*) are attenuated in a murine diabetic wound infection. GBS induces primary and secondary degranulation in primary human neutrophils and the Δ*iagB* mutant is significantly more susceptible to neutrophil killing by cationic antimicrobial peptides and reactive oxygen species than Δ*dltA*. Finally, we found that depletion of neutrophils led to significantly greater bacterial recovery, highlighting the importance of neutrophil defense during diabetic wound infection.

## INTRODUCTION

Diabetes is a group of metabolic diseases, projected to affect over 700 million people by 2045 [1]. A frequent complication of diabetes is the development of wounds on the foot and lower limbs [2,3]. These wounds often become chronic, failing to heal within 4 to 6 weeks, due to an unresolved inflammatory phase [4,5]. This inflammation, primarily driven by neutrophils and macrophages leads to the production of reactive oxygen species (ROS), cationic antimicrobial peptides (CAMPs), matrix metalloproteases, and pro-inflammatory chemokines and cytokines, which perpetuate inflammation and limit the reformation of tissue [6,7].

Diabetic wounds frequently become colonized by a variety of bacterial species which can result in chronic infection [8–11]. While some infections are limited to the wound

itself, if the infection is uncontrolled, bacteria can penetrate deeper tissue leading to bone and systemic infections, which drive the need for amputation [3,12,13]. Some of the most prominent bacterial species identified in diabetic wound infection are

*Staphylococcus aureus*, *Enterococcus faecalis*, Group B *Streptococcus* (GBS), *Pseudomonas aeruginosa* and many anaerobic species [8,9,14,15]. These infections are often difficult to treat due to high levels of antibiotic resistance and tolerance amongst isolates [8,16,17]. Interestingly, work by Sook et al. has demonstrated that *S. aureus* evolves antibiotic resistance in a diabetic host, and that hyperglycemia potentiates the expansion of resistant populations *in vivo* [18]. Further complicating treatment of diabetic wounds is that bacteria in chronic wounds often live in biofilm communities [19,20]. Biofilms, consisting of bacterial cells, DNA, and proteins often lead to a physical barrier which is difficult to treat by antibiotics or routine debridement of tissues [19]. These biofilms can be mono or polymicrobial in nature, and work by Ch'ng et al. has found that *S. aureus* can assist in *E. faecalis* biofilm formation via heme cross-feeding [21].

GBS is a Gram-positive bacterium which colonizes approximately 25% of all individuals in the gastrointestinal and vaginal tract [22–24]. In a healthy host, GBS typically colonizes without any adverse health outcomes; however, GBS can cause urinary tract infections [25] and during pregnancy, GBS can ascend vertically and cause intrauterine infections, leading to inflammation and adverse pregnancy outcomes [26,27]. Further, gestational diabetes mellitus has been identified as a risk factor for increased GBS vaginal colonization [28,29]. In immunocompromised individuals such as neonates, and adults with underlying conditions such as diabetes and cancer, GBS can cause diverse infections including pneumonia, meningitis, cardiovascular disease and sepsis [30–34]. GBS is frequently isolated from diabetic wounds, despite it rarely colonizing the wounds of non-diabetic individuals [11,14,15,35–40]. In addition, GBS alone is sufficient to cause infection and inflammation in the diabetic wound environment [41]. Despite this, little is known about which bacterial factors aid in GBS wound establishment, immune cell evasion, and persistence in this niche.

To address this, we previously developed a murine model of GBS diabetic wound infection and found that GBS infection is exacerbated in a diabetic host when compared to a non-diabetic [41]. RNA-seq on wound tissues revealed that diabetic mice upregulate numerous genes encoding neutrophil effectors such as MPO, elastase, the subunits of calprotectin, as well as pro-inflammatory cytokines and chemokines in response to GBS infection when compared to uninfected controls. We further found that the abundance of these neutrophil effectors was significantly higher in diabetic mice in comparison to non-diabetic upon GBS infection. These data support that GBS encounters high levels of inflammation in the diabetic wound microenvironment, but currently, little is known regarding the bacterial factors that promote survival in this niche. To date only the hemolysin/cytolysin (β-H/C, hemolytic pigment) and the plasminogen binding protein, PbsP, have been shown to contribute to GBS diabetic wound infection [41].

Here, we observe that GBS infection drives an influx of neutrophils into the diabetic wound microenvironment, and that GBS and neutrophils co-localize spatially in diabetic wound tissues. We next utilize a global unbiased approach of transposon sequencing (Tn-seq) and identify GBS genes that are required for fitness in the diabetic wound environment. We find 291 genes that are significantly underrepresented in this niche,

including genes involved in metabolism, capsule biosynthesis, the production of membrane glycolipids and lipoteichoic acid (LTA) alanylation. Membrane lipids are a vital part of host-pathogen interactions [42] and we have recently characterized the role of GBS glycolipids during systemic infection and meningitis disease progression [43–45]. Utilizing GBS glycolipid mutants and a strain deficient in LTA alanylation, we confirm our Tn-seq results by finding that all four mutants are attenuated in diabetic wound infection. We further show the importance of GBS glycolipids and LTA alanylation to keratinocyte interactions and survival against neutrophil killing by cationic antimicrobial peptides (CAMPs) and reactive oxygen species (ROS). Together, these data demonstrate the global gene requirement for GBS fitness in the diabetic wound and further identify GBS glycolipids and LTA alanylation as contributors to neutrophil survival in this niche.

## RESULTS

### *Neutrophils are the most abundant cell type GBS interacts with during diabetic wound infection.*

The diabetic wound is a hyper inflammatory niche with an abundance of immune cells such as phagocytes present [6,46], however, it is unknown which immune cell populations are the most abundant in response to GBS infection. To address this, we wounded diabetic mice and inoculated the wounds with either GBS WT or PBS controls (*n* = 7 per group) and at 48 hpi, euthanized and perfused mice before harvesting wound tissues. We used flow cytometry to quantify different populations of immune cells [47] (Figure S1A). The primary populations of immune cells present in both the uninfected (mock) and GBS infected wounds were neutrophils, followed by macrophages (Figure 1A). Upon infection with GBS, we observed a significant decrease in the numbers of live cells and live $CD45^+$ cells as a percent of collected singlets (Figure S1B,C), suggesting greater cell death, inclusive of immune cells, in the infected wounds compared to uninfected controls. Live neutrophils as a percent of collected singlets did not change between uninfected and infected wounds (Figure S1D); however, neutrophils did represent a greater proportion of immune cells as the percent of neutrophils of live $CD45^+$ cells compared to the mock controls (Figure 1B). Additionally, a significant decrease in the percent of macrophages of live $CD45^+$ cells compared to mock controls was observed (Figure 1B). This suggests that despite increased immune cell death, the remaining live immune cell population is skewed further toward neutrophils in infected wounds. This is consistent with our previous RNA sequencing results that demonstrated a greater abundance of neutrophil effectors such as MPO and elastase, calprotectin, and CXCL1 in GBS infected diabetic wound tissues when compared to uninfected mice [41]. No differences in the $CD11b^-CD11c^-$ (including lymphocytes) and the $MHCII^-SSC^{lo}$ (including monocytes and NK cells) populations as a percent of $CD45^+$ cells were observed (Figure S1E,F). A significant decrease in the percent of $CD24^+$ cells and dendritic cells was observed (Figure S1G,H), possibly due to the proportional increase of neutrophils in the wound. Additionally, we did not observe major alterations in percentages of immune cell populations in the blood of GBS infected and uninfected controls (Figure S1I). These data indicate that neutrophils are the most abundant immune cell type GBS encounters in the wound microenvironment at this time point of infection.

Next, we utilized the same innate immune flow panel to determine which immune cells were present in a non-diabetic vs. a diabetic host during GBS infection (Figure S2). Interestingly, we observed a significant decrease in live cells as percentage of singlets as well as a significant decrease in $CD45^+$ cells as a proportion of live cells in a diabetic host when compared to non-diabetic. These data suggest that the non-diabetic host has more live immune cells in response to GBS infection in the wound (Figure S2A,B). Neutrophils were the most abundant population amongst live cells in both a non-diabetic and diabetic host, highlighting their importance in combatting GBS during wound infection regardless of diabetic status. However, there were significantly more neutrophils in a non-diabetic host than diabetic (Figure S2C,D), and no differences between the other immune populations (Figure S2E-J).

To further confirm the immune profile of diabetic wounds, we utilized multispectral quantitative imaging of wound tissues excised from diabetic mice infected with WT GBS fluorescently tagged with GFP or the mock PBS control. Infected mice developed a robust wound under the epidermal layer (Figure 1C) when compared to the uninfected control. We then chose a region of interest spanning the wound and epidermal layer (boxed in white) for further analysis of immune populations. Pathology of the GBS infected region of interest confirmed a greater proportion of immune cells when compared to the PBS control. GBS co-localized with Ly6G positive cells, confirming the influx of neutrophils to the site of infection (Figure 1D). Conversely, higher levels of F4/80 staining were seen in the PBS control group. These data are the first to demonstrate the spatial dynamics of GBS and immune cells during diabetic wound infection and highlight that GBS and neutrophils interact within this microenvironment.

### *Genome-wide analysis of GBS factors required for survival in the diabetic wound*

We next sought to identify which genetic factors GBS requires to colonize and survive in the diabetic wound. We utilized a GBS Tn mutant library [48–50] in the CJB111 (Serotype V) background [51,52] and our previously described diabetic wound infection model as described in materials and methods [41]. Groups of mice (4 per group) were infected with ~$1.5 \times 10^7$ CFU of the GBS Tn library in biological triplicate. Mice were monitored over the course of infection, and at 48 hours post infection (hpi) mice were euthanized and wound tissue collected (Figure 2A). The input and wound recovered libraries were processed as described in the materials and methods.

To identify transposon insertion sites, sequenced reads were mapped to the GBS CJB111 genome (CP063198) (Figure S3), which identified 291 genes as significantly underrepresented (adj. p-value $< 0.05$, log2FC $< -0.5$) and 213 genes as significantly overrepresented (adj. p-value $< 0.05$, log2FC $> 0.5$) in the wound compared to the input library (Figure 2B) (Table S1). The significant gene hits are distributed across the genome and were then assigned clusters of orthologous groups of proteins (COGs). The number of significant gene hits in each COG were normalized to the total number of genes in each COG, to determine the percentage of genes in each COG that were under- or overrepresented *in vivo*. COGs including nucleotide transport and metabolism, carbohydrate transport and metabolism, inorganic ion transport and metabolism, lipid transport and metabolism, and cell wall/membrane/envelope biogenesis had the greatest

173 proportion of underrepresented genes in the diabetic wound (Figure 2C). We identified
174 multiple genes known to contribute to GBS infection as significantly underrepresented
175 such as genes that are involved in β-H/C biosynthesis, capsule biosynthesis, two-
176 component regulatory systems, glutamine transport, and purine metabolism (Table 1 and
177 Table S1).

**Table 1. Significantly underrepresented genes in the diabetic wound.**

| Locus Tag | Gene | Description | L2FC | Adj. P-Value[a] | Reference |
|---|---|---|---|---|---|
| | | **Virulence Factors** | | | |
| ID870_05935 | *cylA* | ABC transporter ATP-binding protein | -3.66 | 0 | Keogh et al[41] Pritzlaff et al[53] Armistead et al[54] |
| ID870_05930 | *cylB* | ABC transporter permease | -2.03 | 0 | |
| ID870_05910 | *cylJ* | cylJ protein | -0.92 | 0 | |
| ID870_05925 | *cylE* | cylE protein | -0.9 | 0 | |
| ID870_05950 | *cylG* | 3-oxoacyl-ACP reductase | -0.88 | 0.0008 | |
| ID870_05905 | *cylK* | CylK protein | -0.78 | 0 | |
| ID870_05915 | *cylI* | beta-ketoacyl-[acyl-carrier-protein] synthase family protein | -0.61 | 0 | |
| ID870_05340 | *sodA* | superoxide dismutase | -1.91 | 0 | Rajagopal et al[55] |
| ID870_05245 | *prsA* | peptidylprolyl isomerase | -1.52 | 0 | |
| ID870_03375 | *hylB* | hyaluronate lyase | -0.79 | 0 | Kolar et al[56] |
| ID870_07370 | *perR* | peroxide-responsive transcriptional repressor PerR | -0.61 | 0.04178 | Dubbs et al[57] |
| ID870_04625 | *srtA* | class A sortase | -1.06 | 0 | Lalioui et al [58] |
| ID870_04175 | *esxA2* | WXG100 family type VII secretion target | -0.85 | 0.03819 | Spencer et al[59] |
| ID870_04190 | *esaB* | EsaB/YukD family protein | -1.35 | 0.03125 | |
| ID870_04220 | - | hypothetical protein - transmembrane | -0.73 | 0.04834 | |
| ID870_04265 | - | hypothetical protein | -0.64 | 0.00153 | |

| | | | | | |
|---|---|---|---|---|---|
| ID870_04290 | - | T7SS lipoprotein protein | -0.73 | 0 | |
| **TCS systems** | | | | | |
| ID870_05670 | TCS8_S/*vicK* | cell wall metabolism sensor histidine kinase VicK | -2 | 0 | Faralla et al[60] Thomas et al[61] |
| ID870_03010 | TCS12_S | HAMP domain-containing histidine kinase | -1.44 | 0 | Faralla et al[60] Thomas et al[61] |
| ID870_04455 | *ciaR* | response regulator transcription factor | -1.31 | 0 | Quach et al[62] Spencer et al [63] |
| ID870_04460 | *ciaH* | HAMP domain-containing histidine kinase | -1.02 | 0 | |
| ID870_10425 | TCS19_R | response regulator transcription factor | -0.86 | 0.00766 | Faralla et al[60] Thomas et al[61] |
| ID870_05710 | TCS7_R | response regulator transcription factor | -0.59 | 0.03302 | Faralla et al[60] Thomas et al[61] |
| **Capsule/Cell wall/membrane** | | | | | |
| ID870_00715 | *dltX* | teichoic acid D-Ala incorporation-associated protein | -1.68 | 0.03105 | Poyart et al[64] Poyart et al [65] |
| ID870_00725 | *dltB* | D-alanyl-lipoteichoic acid biosynthesis protein | -2.6 | 0 | |
| ID870_00730 | *dltC* | D-alanine--poly(phosphoribitol) ligase subunit | -1.73 | 0.01571 | |
| ID870_03480 | *cpsY* | LysR family transcriptional regulator | -2.83 | 0 | Noble et al[66] Carlin et al[67], Uchiy |
| ID870_03550 | *cpsL* | oligosaccharide flippase family protein | -1.78 | 0 | |
| ID870_03560 | *neuC* | UDP-N-acetylglucosamine 2-epimerase | -0.58 | 0.01066 | |

| | | | | | |
|---|---|---|---|---|---|
| ID870_03570 | *neuA* | N-acylneuraminate cytidylyltransferase | -0.72 | 0.00463 | ama et al [68] |
| ID870_05455 | *pbp2b* | penicillin-binding protein 2 | -1.68 | 0 | |
| ID870_08625 | *pbp1B* | penicillin-binding protein | -0.85 | 0 | |
| ID870_08710 | *pbp3* | D-alanyl-D-alanine carboxypeptidase | -0.98 | 0 | |
| ID870_05725 | *iagA* | glycosyltransferase | -4.87 | 0 | Doran et al[45] |
| ID870_07565 | *accD* | acetyl-CoA carboxylase carboxyltransferase subunit beta | -1 | 0.04354 | |
| ID870_07575 | *fabZ* | 3-hydroxyacyl-ACP dehydratase | -1.85 | 0.03968 | |
| ID870_07610 | *fabH* | ketoacyl-ACP synthase III | -1.51 | 0 | |
| ID870_08755 | *uppP* | undecaprenyl-diphosphate phosphatase | -0.73 | 0 | |
| ID870_10050 | *mprF* | bifunctional lysylphosphatidylglycerol flippase/synthetase MprF | -0.73 | 0 | Joyce et al[44] |
| | | ***Metabolism*** | | | |
| ID870_00505 | *ahpC* | peroxiredoxin | -2.32 | 0 | |
| ID870_00585 | *purA* | adenylosuccinate synthase | -6 | 0 | Rajagopal et al[69] |
| ID870_00850 | *glnR* | MerR family transcriptional regulator | -1.67 | 0.01484 | |
| ID870_01300 | *manA* | mannose-6-phosphate isomerase class I | -0.79 | 0.04253 | |
| ID870_02315 | *glnQ* | amino acid ABC transporter ATP-binding protein | -1.47 | 0 | Tamura et al[70] |
| ID870_02320 | *glnP* | ABC transporter substrate-binding protein/permease | -1.17 | 0 | |
| ID870_04130 | *pyrF* | orotidine-5'-phosphate decarboxylase | -3.4 | 0 | |
| ID870_04135 | *pyrE* | orotate phosphoribosyltransferase | -1.54 | 0 | |
| ID870_04145 | *pyrB* | aspartate carbamoyltransferase catalytic subunit | -1.86 | 0 | |
| ID870_04150 | *carA* | glutamine-hydrolyzing carbamoyl-phosphate synthase small subunit | -1.13 | 0.00215 | |
| ID870_04155 | *carB* | carbamoyl-phosphate synthase large subunit | -1.28 | 0 | |

| | | | | | |
|---|---|---|---|---|---|
| ID870_04545 | *guaA* | glutamine-hydrolyzing GMP synthase | -6.78 | 0 | Rajagopal et al[69] Ipe et al [71] |
| ID8_05480 | *ppc* | phosphoenolpyruvate carboxylase | -2.51 | 0 | |
| ID870_07185 | *nrdE* | class 1b ribonucleoside-diphosphate reductase subunit alpha | -1.42 | 0 | |
| ID870_07190 | *nrdI* | class Ib ribonucleoside-diphosphate reductase assembly flavoprotein NrdI | -1.14 | 0 | |
| ID870_07195 | *nrdF* | class 1b ribonucleoside-diphosphate reductase subunit beta | -2.16 | 0 | |
| ID870_07535 | *manN* | PTS mannose/fructose/sorbose transporter family subunit IID | -0.98 | 0 | |
| ID870_07540 | *manO* | DUF956 family protein | -1.52 | 0.04152 | |
| ID870_09305 | *purB* | adenylosuccinate lyase | -7.52 | 0 | Rajagopal et al[69] |
| ID870_09315 | *purK* | 5-(carboxyamino)imidazole ribonucleotide synthase | -1.46 | 0.00522 | |
| ID870_09320 | *purE* | 5-(carboxyamino)imidazole ribonucleotide mutase | -2.44 | 0 | |
| ID870_09325 | *purD* | phosphoribosylamine--glycine ligase | -3.05 | 0 | |
| ID870_09390 | *purH* | Bifunctional phosphoribosylaminoimidazolecarboxamide formyltransferase/IMP cyclohydrolase | -3.74 | 0 | |
| ID870_09400 | *purN* | phosphoribosylglycinamide formyltransferase | -3.43 | 0 | |
| ID870_09405 | *purM* | phosphoribosylformylglycinamidine cyclo-ligase | -2.91 | 0 | |
| ID870_09410 | *purF* | amidophosphoribosyltransferase | -1.54 | 0 | |
| ID870_09420 | *purC* | Phosphoribosylaminoimidazolesuccinocarboxamide synthase | -4.15 | 0 | |
| ID870_09800 | *guaB* | IMP dehydrogenase | -3.11 | 0 | Rajagopal et al[69] Ipe et al [71] |

| | | | | |
|---|---|---|---|---|
| ID870_10270 | *nrdD* | anaerobic ribonucleoside-triphosphate reductase | -1.16 | 0 |
| ID870_10290 | *nrdG* | anaerobic ribonucleoside-triphosphate reductase activating protein | -1.2 | 0.00279 |

[a] Adj. P-Value <0.0001 is assigned 0 by TRANSIT.

Interestingly, among the most significantly underrepresented genes was *iagA* (Figure 2D, Table 1) which is a glycosyltransferase involved in the biosynthesis of the LTA anchor, diglucosyl-diacylglycerol ($Glc_2$-DAG) in GBS [43,45] (Figure 2E), and is in an operon with the first glycolipid biosynthesis gene, *iagB*, that is responsible for glucosyl-DAG (Glc-DAG) biosynthesis [43]. An additional gene in glycolipid biosynthesis pathway, *mprF* responsible for synthesizing the amino acylated glycolipid lysyl-glucosyl-DAG (Lys-Glc-DAG) [44,72] and multiple genes involved in the alanylation of LTA (*dlt* operon) [65] were also significantly underrepresented in the diabetic wound compared to input (Figure 2D,E). The two remaining genes in the biosynthetic pathway, namely *iagB* and *ltaS* genes, were not identified in the Tn-seq dataset. However, upon further investigation, we observed that there were very few to no transposon insertions present in these genes in the input libraries, thus making it hard to identify their importance with this approach. GBS glycolipids have recently been shown to impact GBS bloodstream survival [43] and disruption and inflammation of the blood-brain barrier (BBB) [44,45], while alanylation of LTA has been shown to be important for bloodstream survival [64]; yet the contribution of these pathways to GBS survival in the diabetic wound have yet to be elucidated.

***GBS glycolipids and LTA alanylation are required for epithelial cell invasion and survival in the diabetic wound.***

To colonize the diabetic wound, GBS must interact with epidermal keratinocyte cells, a highly specialized epithelial cell [73]. To investigate the direct interaction between GBS WT CJB111 as well as isogenic glycolipid mutants in *iagB*, [43], *iagA* [43], *mprF* [44] and *dltA* and human keratinocytes, we used the immortalized human keratinocyte cell line, N/TERT-2G [74]. GBS∆*iagB* is devoid of all glycolipids, GBS∆*iagA* lacks $Glc_2$-DAG the LTA anchor, GBS∆*mprF* lacks the lysine decorated lipids Lys-Glc-DAG and Lys-PG, and the GBS∆*dltA* mutant is unable to add alanine modifications to its LTA polymer [65] (Figure 2E). *In vitro* assays for adhesion and invasion were performed as described previously for other cell lines [63,75]. There was no significant difference in the ability of the mutant strains to adhere to N/TERT cells (Figure 3A); however, there were significantly fewer mutant bacteria recovered from the intracellular compartment compared to GBS WT (Figure 3B) indicating GBS glycolipids and LTA alanylation may play roles in invasion of human keratinocytes. Furthermore, it was observed that GBS∆*iagB* has significantly reduced intracellular survival over time compared to GBS WT, whereas all other mutant strains survived like GBS WT (Figure 3C). These observations indicate GBS glycolipids and LTA alanylation may contribute to GBS persistence in the wound.

To assess if there were alterations to the cell envelope of the mutants that may impact their interactions with keratinocytes, we performed transmission electron microscopy (TEM) (Figure S4A). We observed that GBS∆*iagB* appears to have a general thickening of the cell envelope, along with GBS∆*mprF* appearing to have minor thickening as well. GBS∆*iagA* has no difference in appearance compared to GBS WT. Interestingly, GBS∆*dltA* has a significantly altered inner electron dense ring compared to GBS WT and the other mutants, confirming prior work by Saar-Dover *et al*.[76] In general all strains retained the polysaccharide capsule as assessed by flow cytometry using anti-sera targeting the type V capsule (Figure S4B). Interestingly, both GBS∆*iagB* and GBS∆*iagA* exhibited a slight, but significant, increase in capsule abundance compared to WT, which was restored to WT levels in the complemented strains. Additionally, no difference in membrane fluidity was observed between all strains as measured by anisotropy (Figure S4C).

To confirm our Tn-seq results and to elucidate the role of glycolipids and LTA alanylation during diabetic wound infection, we utilized our established streptozotocin induced diabetic wound model of infection [77] with GBS WT CJB111, ∆*iagB*, ∆*iagA*, ∆*mprF* and *dltA* mutant strains. After 48 hpi, all mutants were significantly attenuated in comparison to WT GBS (Figure 3D). Notably, in addition to having reduced bacterial burden in the wound, mutant strains were not able to spread systemically compared to WT GBS as evidenced by significantly reduced recovery of mutant bacteria from the kidneys (Figure 3E). Additionally, far fewer mice had detectable CFU in the kidneys compared to WT infected mice (Figure 3F). These data indicate that GBS glycolipids and LTA alanylation play an important role in GBS wound survival and systemic spread during diabetic infection.

Next, we assessed how GBS glycolipids and LTA modification would impact the abundance of neutrophil chemoattractant, CXCL1, and the leukocyte-derived enzyme myeloperoxidase (MPO) in the diabetic wound at the endpoint of infection. Wounds from mice infected with GBS∆*iagB* and GBS∆*iagA* had a significant decrease in both CXCL1 compared to GBS WT whereas wounds infected with GBS∆*mprF* and GBS∆*dltA* had no significant difference in CXCL1 abundance (Figure 3F). Interestingly, only GBS∆*iagA* infected wounds had a significant decrease in the abundance of MPO compared to GBS WT infected wounds, suggesting high levels of neutrophils were still present in the GBS∆*iagB,* GBS∆*mprF,* and GBS∆*dltA* wounds to combat the infection (Figure 3G). We next utilized an early time point (5 hpi), to determine whether the loss of glycolipids impacted the influx of neutrophils to the site of infection. Mice infected with either WT, GBS∆*iagB* (to determine impact of all glycolipids) and GBS∆*dltA,* showed similar CFU recovery and abundance of CXCL1 and MPO (Figure S5). These data suggest that WT and mutant strains encounter similar levels of neutrophils early in infection and that the enhanced susceptibility of the GBS∆*iagB* and GBS∆*dltA* mutants to neutrophil killing led to enhanced clearance by 48 h.

**GBS glycolipids and LTA alanylation are vital for surviving neutrophil killing.**

To further understand the interaction between GBS and neutrophils, we isolated primary human neutrophils from four independent donors (two female and two male) to

assess primary human neutrophil killing of GBS in diabetic glucose levels. Primary human neutrophils were conditioned in media containing 22 mM glucose to mimic hyperglycemia [46] before being exposed to opsonized bacteria. To assess the role of all GBS glycolipids, including the LTA anchor, we used a GBS∆*iagB* mutant and to assess impact of LTA alanylation we used the GBS∆*dltA* mutant. A significant decrease in survival was observed for GBS∆*iagB* compared to GBS WT, which is consistent to our previous study [43] of GBS∆*iagB* susceptibility to neutrophil killing under non-diabetic conditions; however, no significant difference was observed between GBS∆*dltA* and GBS WT (Figure 4A). The phenotype of the GBS∆*iagB* mutant was rescued when the strain was complemented with a plasmid containing the *iagB* gene *(*+pJIagB). GBS∆*dltA* is known to be more susceptible to neutrophil killing and bloodstream clearance [64] so we assessed opsonophagocytic neutrophil mediated killing over time using the human HL60-neutrophil like cell line that is routinely maintained and differentiated in high glucose media. Interestingly, we observed that GBS∆*iagB* is significantly more susceptible to neutrophil killing at 1, 2 and 3 h compared to GBS WT, whereas only after 2 and 3 h of infection was there a significant difference between GBS∆*dltA* and GBS WT (Figure 4B). Additionally, after 3 h of exposure there was less than 1% survival for both mutants whereas WT maintains approximately 15% survival. These data indicate that GBS glycolipids and LTA alanylation both contribute to thwarting neutrophil clearance.

Since GBS∆*iagB* and GBS∆*dltA* are more susceptible to neutrophil killing, we next assessed if these mutants exhibited an altered phagocytic uptake compared to WT using imaging flow cytometry. Opsonized GFP-labelled GBS WT, GBS∆*iagB*, and GBS∆*dltA* were exposed to HL60 cells for 15 minutes. Interestingly, we observed a significantly higher percent of GFP-positive cells when incubated with GBS∆*iagB* compared to WT and GBS∆*dltA* (Figure 4C). We next assessed how many bacteria are present in each cell that was GFP positive (Figure 4D,E) and observed GBS WT had more low numbers (1-2 GBS per cell) compared to the mutant strains, whereas GBS∆*iagB* and GBS∆*dltA* had significantly higher numbers (3 or more GBS/cell) compared to WT. Representative images are shown in Figure 4F. Interestingly, over 80% of GFP positive HL60s had GBS both inside and membrane associated compared to the inside or membrane only location, confirming phagocytosis of GBS (Figure S5D-F). These data demonstrate that the loss of GBS glycolipids results in higher frequency in phagocytosis, which along with the loss of LTA alanylation results in increased bacteria per neutrophil.

***Glycolipids contribute to GBS survival against CAMPs and ROS.***

Neutrophils utilize multiple antimicrobial components to kill bacteria, especially CAMPs such as cathelicidin and ROS such as hydrogen peroxide and hypochlorite [78–81]. The alanylation of LTA has previously been shown to contribute to GBS evasion of CAMPs by regulating the density of the cell wall [64]. Similarly, we have recently demonstrated that all three GBS glycolipids aid in the protection against CAMP-mediated killing, likely through a charge repulsion mechanism [43]. Here, we observed GBS∆*iagB* is more susceptible to neutrophil killing compared to GBS WT and to GBS∆*dltA*. To assess if the same is true with CAMP susceptibility, empty vector strains of GBS WT, GBS∆*iagB*, GBS∆*dltA*, and complement strains GBS∆*iagB*+pJIagB and GBS∆*dltA*+pJDltA were incubated with 20 µM of the mouse cathelicidin, mCRAMP, for 30 min. We observed that

305 the GBS∆*iagB* mutant exhibited significantly more mCRAMP sensitivity compared to GBS
306 WT and GBS∆*dltA* strains, and the complemented strains restored survival to WT levels
307 (Figure 4C). Possible explanations for this difference in CAMP susceptibility are
308 alterations in membrane fluidity [82]. However, no difference in membrane fluidity was
309 observed between all strains as measured by anisotropy, indicating CAMP susceptibility
310 is independent of membrane fluidity in these mutants (Figure S4C).

311 ROS is another major mechanism of bacterial killing employed by neutrophils and
312 diabetic wounds have increased levels of ROS compared to nondiabetic wounds [83,84];
313 thus, we hypothesized that glycolipids and LTA alanylation would contribute to ROS
314 survival. To investigate this, empty vector strains of GBS WT, GBS∆*iagB*, GBS∆*dltA*, and
315 complement strains GBS∆*iagB*+pJIagB and GBS∆*dltA*+pJDltA were incubated with
316 0.08% hypochlorite (HOCl) for 1 h resulting in a significant decrease in survival of the
317 GBS∆*iagB* mutant compared to GBS WT, which was rescued to WT survival levels in the
318 GBS∆*iagB*+pJIagB complement strain (Figure 4D). No difference in survival was
319 observed between GBS∆*dltA,* GBS∆*dltA*+pJDltA, and GBS WT. To further confirm ROS
320 susceptibility and assess oxidative DNA damage; GBS WT, GBS∆*iagB* and GBS∆*dltA*
321 were exposed to 100 µg of hydrogen peroxide for 1 h resulting in a significant decrease
322 in survival of the GBS∆*iagB* mutant compared to GBS WT. No difference between GBS
323 WT and GBS∆*dltA* was observed (Figure 4E). Similarly, we measured oxidative DNA
324 damage via ELISA and observed a significant increase in fold change of oxidative DNA
325 damage in the GBS∆*iagB* strain compared to untreated, GBS WT, and GBS∆*dltA* strains
326 (Figure 4F). No difference was observed between GBS∆*dltA* and GBS WT or untreated
327 cells. These data suggest that LTA alanylation is important for resisting CAMPs; however,
328 GBS glycolipids promote resistance to both CAMPs and ROS.

329

330 ***GBS induces primary and secondary degranulation in primary human neutrophils***

331 An important mechanism of neutrophil killing of bacteria is degranulation.
332 Neutrophils produce four types of granules: azurophilic/primary, specific/secondary,
333 gelatinase/tertiary and secretory, with high concentrations of CAMPs, ROS, proteinases
334 and additional antimicrobial factors harbored in the primary and secondary granules [78–
335 81]. To assess induction of degranulation we exposed primary human neutrophils
336 conditioned in media containing 22 mM glucose to mimic hyperglycemia to opsonized
337 GBS WT, GBS∆*iagB* and GBS∆*dltA* for 30 min and assessed degranulation using flow
338 cytometry for established human degranulation markers [85] (Figure S3B). We observed a
339 significant increase in azurophilic/primary degranulation, indicated by the increased
340 surface expression of CD63 (Figure 5A) and specific/secondary degranulation, indicated
341 by the increased surface expression of CD66b (Figure 5B) and CD15 (Figure S6B), of
342 neutrophils exposed to GBS regardless of the GBS strain, compared to uninfected control
343 neutrophils. Interestingly, the GBS∆*iagB* mutant, even though more susceptible to ROS
344 and CAMPs, induces significantly higher levels of azurophilic/primary degranulation
345 compared to GBS WT and GBS∆*dltA* mutant. While GBS infection resulted in no
346 difference in surface expression of gelatinase/tertiary degranulation marker CD11b
347 between infected and uninfected neutrophils, we did observe an increase in surface CD18
348 expression on infected neutrophils compared to uninfected neutrophils, suggesting
349 tertiary degranulation is not stimulated or is stimulated to a lesser extent (Figure S6C).

350 These data indicate that neutrophils recognize GBS, regardless of the missing glycolipids
351 or LTA alanylations, and trigger primary and secondary degranulation to combat them.

352

353 ***Neutrophils influence GBS burden in the wound and kidneys of diabetic mice.***

354 Neutrophils are highly abundant during diabetic wound infection and promote high
355 inflammation in the microenvironment [46,86], as we have also observed during GBS
356 infection (Figure 1). We therefore sought to investigate the contribution of neutrophils to
357 GBS clearance in a diabetic host, and we hypothesized that depletion of neutrophils in
358 the diabetic wound would lead to enhanced recovery of the GBS∆*iagB* and GBS∆*dltA*
359 mutants in comparison to non-depleted controls. To investigate this, systemic neutrophil
360 depletion of diabetic mice was performed via intraperitoneal injection of anti-Ly6G
361 antibody, and non-depleted mice were injected with isotype (anti-IgG2a antibody) control
362 one day before infection. Neutrophil depletion in wound tissues was confirmed by flow
363 cytometry (Figure S7A,B). Neutrophil depleted and control diabetic mice were infected
364 with either GBS WT, GBS∆*iagB* or GBS∆*dltA* mutants using our streptozotocin induced
365 diabetic wound infection model. Depletion of neutrophils lead to a significant increase
366 bacterial burden of GBS WT and GBS∆*iagB* as well as an increase in GBS∆*dltA* in the
367 diabetic wound compared to the non-depleted controls at 48 hpi (Figure 6A). While GBS
368 burdens were consistently higher in depleted compared to non-depleted controls, the
369 GBS∆*iagB* and GBS∆*dltA* mutants still exhibited a decreased burden when compared to
370 GBS WT within the neutrophil depleted group (Figure 6A). Similarly, depletion of
371 neutrophils in non-diabetic mice resulted in significantly higher recovered CFU and
372 greater weight loss in the depleted group vs control (Figure S7C,D). Depletion of
373 neutrophils in diabetic mice also led to greater GBS dissemination into the kidneys based
374 on CFU recovered (Figure 6B). Interestingly, significant increases in bacterial burdens in
375 the kidneys of depleted mice infected with GBS∆*iagB* and GBS∆*dltA* compared to non-
376 depleted mice was observed and a higher percentage of mice had CFU in the kidneys in
377 the depleted groups vs non-depleted groups (Figure 6C). Taken together these data
378 indicate that neutrophils play an important role in controlling GBS persistence in the
379 wound and preventing systemic spread in the diabetic host. They further suggest that
380 circulating neutrophils can control both the GBS∆*iagB* and GBS∆*dltA* during invasive
381 infection *in vivo*.

382

383 **DISCUSSION**

384 The diabetic wound is hyperinflammatory, with high levels of neutrophils and
385 macrophages potentiating inflammation and limiting reformation of the extracellular matrix
386 [87]. However, prior to this work it was unknown how the presence of GBS in diabetic wound
387 infection would affect immune cell populations. Using flow cytometry, we found that
388 neutrophils are the most abundant immune cell GBS encounters during initial diabetic
389 wound infection (48 hpi), making up greater than 65% of all immune cells. We also found
390 a significant increase in the percentage of neutrophils residing in the diabetic wound
391 infected with GBS compared to uninfected controls. We then compared the immune
392 populations in GBS infected wounds in a healthy and a diabetic host. While neutrophils
393 were the most abundant population regardless of host status, we saw a significant

394 decrease in the percentage of live immune cells in diabetic mice, suggesting GBS may
395 be killing immune cells at a greater level in a host with diabetes. In addition to flow
396 cytometry, we performed multispectral immunohistochemistry on GBS and mock infected
397 wounds to visualize the localization of both GBS and immune cells during diabetic wound
398 infection. Wounds infected with GBS led to the formation of a large bolus of bacteria within
399 the wound underneath the area of initial incision. This area contained GBS that seemed
400 to co-localize with neutrophils at the wound site. This was not the case for all immune
401 populations as macrophages were more present in the tissue section from mock infected
402 wounds in comparison to GBS infected. These data are the first to spatially characterize
403 the GBS-host interactions within diabetic wound infection and demonstrate the proximity
404 of neutrophils and the bacterium within the wound. Further, it highlights the need for
405 mechanistic studies that identify GBS factors that contribute to neutrophil survival in this
406 niche.

407 Despite the growing evidence that GBS is present in diabetic wound infections,
408 little is known about the genetic factors required for fitness and survival in the wound.
409 Here, we used a highly saturated Tn-seq library and identified 291 significantly
410 underrepresented genes in diabetic wound infection, indicating they may be required for
411 fitness. One of the most significantly underrepresented genes was *iagA*, which encodes
412 for an enzyme involved in GBS glycolipid biosynthesis and is responsible for synthesizing
413 the LTA anchor, $Glc_2$-DAG, [43,45]. Additionally, multiple genes encoding enzymes involved
414 in the alanylation of GBS LTA were significantly under-represented [65], suggesting that
415 both LTA anchoring and modification are important for GBS to establish itself in this niche.
416 Further investigation of the dataset identified *mprF,* another gene in the GBS glycolipid
417 biosynthesis pathway, and the enzyme responsible for lysinylation of Glc-DAG and
418 phosphatidylglycerol [44]. Two genes in these biosynthetic pathways (*iagB* and *ltaS*) were
419 not identified in our Tn-seq screen, however, very few transposon insertions in these
420 genes were present in the input library. *LtaS* is known to be essential in other Gram-
421 positive bacteria [88,89]; however, *iagB* is not essential thus highlighting a limitation of
422 largescale datasets and potential for false negative hits. In this work, we characterize the
423 role of GBS glycolipids and the alanylation of LTA in diabetic wound infection. Using our
424 isogenic glycolipid mutants (Δ*iagB,* Δ*iagA,* Δ*mprF*) and our newly constructed LTA
425 alanylation mutant (Δ*dltA*), we confirmed our Tn-seq results observing significant
426 attenuation of these mutants in the diabetic wound compared to GBS WT 48 hpi
427 Throughout this work, we focused on the mechanisms by which all GBS glycolipids and
428 LTA modification contribute to survival in the diabetic wound using the GBSΔ*iagB* (lacking
429 all glycolipids) and GBSΔ*dltA* (unable to add alanine modifications to LTA) mutant strains.
430 Analysis of these mutants at an early time point (5 hpi) revealed that CFU was similar
431 between all strains, demonstrating that these mutants are able to establish infection and
432 are cleared between 5 and 48 h. Further, levels of MPO and CXCL1 were similar in all
433 infected tissues suggesting that immune cells are called to the site of infection at a similar
434 rate. Further we show that complementation of GBSΔ*iagB* in the diabetic wound restores
435 CFU to GBS WT levels (Figure S7E).

436 Little is known about GBS interaction with keratinocytes, with the only factor known
437 to aid adherence to keratinocytes being the adhesin, PbsP [41]. Interestingly, we observed
438 the GBS glycolipids and LTA alanylation do not play a role in adherence to human
439 keratinocytes but are important for invasion into the intracellular compartment, as has

been observed previously for the BBB endothelial cells [43–45]. Further, we found that the GBS∆*iagB* mutant had reduced intracellular survival over two hours of incubation with keratinocytes when compared to WT and other strains. These data suggest that all the glycolipids together contribute to survival once inside keratinocytes. The glycolipid mutant, GBS∆*mprF,* is more susceptible to low pH compared to GBS WT [44] highlighting the glycolipid mutants may be more susceptible to lysosomal killing compared to GBS WT once inside the host cell. It is currently unknown what receptors GBS binds to on keratinocytes, the mechanisms of invasion, and additional GBS factors such as membrane vesicles that may promote invasion into the intracellular compartment of keratinocytes. Thus, further investigation into the mechanisms of interactions of GBS and keratinocytes are warranted, as this may serve as a mechanism to escape from immune cells in the wound and act as potential reservoirs for persistence colonization of the diabetic wound after debridement of the wound.

We have previously found that GBS glycolipids are important for survival against neutrophils, as strains lacking glycolipids have enhanced susceptibility to antimicrobial peptides. However, these studies were performed with neutrophils cultured in normoglycemic levels of glucose. Individuals with diabetes are known to have aberrant neutrophil function, largely driven by hyperglycemia [90]. We therefore cultured neutrophils in media containing levels of glucose that are physiologically relevant in a diabetic host to assess the role of GBS glycolipids and LTA alanylation to neutrophil survival in high glucose conditions. Interestingly, we observed GBS∆*iagB* is phagocytized at a higher frequency than GBS WT and GBS∆*dltA* and both mutants had higher number of GBS per neutrophil compared to GBS WT. These observations demonstrate that GBS glycolipids are important for preventing uptake by neutrophils and once engulfed, important for protecting against killing mechanisms. Here, we also focused on a second mechanism of neutrophil killing, degranulation, using our glycolipid devoid strain, GBS∆*iagB*, and our LTA alanylation mutant, GBS∆*dltA*. Using primary human neutrophils exposed to high glucose conditions, we observed all GBS strains, regardless of mutation, triggered both primary and secondary degranulation. This suggests that the mechanism by which neutrophils recognize GBS and elicit degranulation is not dependent on GBS glycolipids or LTA modification. Neutrophil granules, particularly the primary/azurophilic and secondary/specific granules, harbor a variety of antimicrobial properties such as CAMPs and ROS. Due to the hyperglycemia in diabetic individuals, neutrophils are transcriptionally primed to undergo NETosis [46]. Work by Derré-Bobillot et al. identified a secreted GBS nuclease, NucA involved in the degradation of the DNA matrix, or major backbone of NETs [46,91]. Further, our group has found that this nuclease is highly upregulated in bacteria recovered from the diabetic wound in comparison to input [41]. NucA was not identified in the Tn-seq screen, likely because it is a secreted factor that the rest of the population is still producing, preventing it from being underrepresented; however, it may be important in the diabetic wound microenvironment, and its contribution to GBS survival in the diabetic wound is ongoing.

Cationic antimicrobial peptides such as cathelicidin and defensins are small peptides used by the host to target invading pathogens and are an important antimicrobial factor in neutrophil granules. We and others have shown that GBS glycolipids and LTA alanylation are important for resisting CAMP mediated killing although potentially via different mechanisms [43,64,76]. Saar-Dover *et al* observed that both GBS∆*dltA* and

GBS∆*mprF* have a more negatively charged cell surface; however, the *mprF* mutant is not susceptible to CAMPs [76]. Interestingly, they observed the GBS∆*dltA* has a significantly altered cell wall density resulting in CAMP susceptibility. Based on TEM images here and our previous study, we identified the GBS∆*iagB* mutant has a significantly more negatively charged cell membrane compared to GBS WT, suggesting the susceptibility to CAMPs is via different mechanism[43]. Interestingly we observed that GBS∆*iagB* was significantly more attenuated than the GBS∆*dltA* after 30 min of exposure to mouse cathelicidin, even though the membrane fluidity is the same between these mutants and GBS WT. A possible explanation is that while the alanylation of LTA is required for proper cell wall density to mediate CAMP resistance[76], the loss of the glycolipids, including the LTA anchor, results in a more severe change in cell wall dynamics possibly making the membrane hyper-attractive to the positively charged CAMPs. Another major antimicrobial property of neutrophil granules is the production of ROS, especially hydrogen peroxide which is used by myeloperoxidase to generate hypochlorite. Not only do neutrophils generate high amounts of ROS, but the diabetic wound contains a large amount of ROS compared to non-diabetic wounds [83,84]. Like the CAMP phenotype, we observed GBS devoid of glycolipids is more susceptible to both hypochlorite and hydrogen peroxide killing and resulting oxidative DNA damage compared to both WT and ∆*dltA* mutant. This could be due to increased lipid peroxidation of the cellular membrane lacking glycolipids which may generate even more ROS, resulting in increased damage to the cell and death [92], but further investigation is needed to identify why glycolipids may protect against ROS attack.

Among the significantly underrepresented genes identified in this Tn-seq are multiple factors required for metabolism such as purine metabolism, glutamine metabolism, and mannose utilization. These genes are important for bacterial pathogenesis [93] and were recently identified to be important for *Enterococcus* colonization of non-diabetic wounds [94]. We also identified multiple GBS virulence factors such as the β-H/C *cyl* operon and the type VII secretion system (T7SS) as under-represented in the diabetic wound. The loss of the GBS β-H/C has been previously shown to impact bloodstream survival and phagocytic defense, and we have also observed its importance to diabetic wound persistence [41,95]. Similarly, the role of the T7SS has recently been implicated in cytotoxicity to host cells and promotes colonization of the vaginal tract [59,96]. With the high number of neutrophils and macrophages present in the diabetic wound the T7SS may have important functions for defending against these immune cells and potentially against other bacterial species that colonize this polymicrobial environment. Interestingly, multiple two component systems (TCS) were significantly underrepresented in the Tn-seq. One such TCS, CiaH/R has been implicated in monitoring cell wall/surface stress [62,97]. GBS TCS 8, which has homology to the VicR/K (WalR/K in some species) system in other streptococci was also significantly underrepresented [61,98]. Interestingly three currently uncharacterized TCS systems, TCS 7, 12 and 19 [61] were also significantly underrepresented. The fact that these TCS systems were significantly underrepresented suggests the strong need for GBS adaptation to the diabetic wound microenvironment. It further suggests these TCS systems may play a pivotal, currently unknown, role in GBS niche adaption, which requires further investigation.

Overall, using Tn-seq, this work has identified multiple GBS factors that are required to colonize the diabetic wound and to evade the large number of immune cells present there (Figure 7). Neutrophils are important first line responder to invading pathogens and the ability for GBS to evade the multiple killing mechanism they possess is vital to establishment in this niche. The characterization of the role that GBS glycolipids and LTA alanylation play during colonization of the wound and evasion of neutrophil killing highlights important cell wall properties that could be targeted by small molecules to aid in the clearance of GBS. Future studies aim to elucidate the roles of other genetic factors identified in the Tn-seq and their contribution to diabetic wound colonization. Ultimately, this work will provide increased knowledge of GBS pathogenesis and virulence potential, aiding in future treatments and may have broad implications to other bacterial species that may colonize the diabetic wound.

## ACKNOWLEDGMENTS

The authors would like to thank the members of the Doran and Horswill labs for constructive discussions in the preparation of this manuscript, Dr. Robb Welty at the Biophysics Shared Research Facility at the University of Colorado Anschutz Medical Campus for help with anisotropy experiments, the Electron Microscopy Core Facility at the University of Colorado Anschutz Medical Campus for help with TEM and the Human Immune Monitoring Shared Resource, specifically Troy Schedin and Angela Minic within the University of Colorado Cancer Center (P30CA0434) for their expert assistance in analysis of diabetic wound tissues. This work was funded in part by the American Heart Association grant 23POST1013835 to L.R.J, NIH/NIAID F31AI178881 to M.S.A, F32AI172126 and K99AI180373-02 to R.A.K., R21AI171853 to K.S.D and A.R.H, R01AI178692 to K.S.D.

## AUTHOR CONTRIBUTIONS

Conceptualization: LRJ, KSD, RAK; Methodology: LRJ, MSA, DTN, BLS, RAK; Validation: LRJ, MSA, DTN, BLS, JK, KSD, RAK ; Formal analysis: LRJ, MSA, DTN, JK, RAK; Investigation: LRJ, MSA, DTN, RAK; Resources: JK, KSM, ARH, KSD; Writing original draft: LRJ, RAK; Editing and reviewing: LRJ, MSA, DTN, BLS, JK, KSM, ARH, KSD, RAK; Visualization: LRJ, DTN, RAK; Project administration: LRJ, KSD, RAK; Funding acquisition: LRJ, KSM, ARH, KSD, RAK

## DECLARATION OF INTERESTS

The authors declare no competing interests

567 **FIGURES**

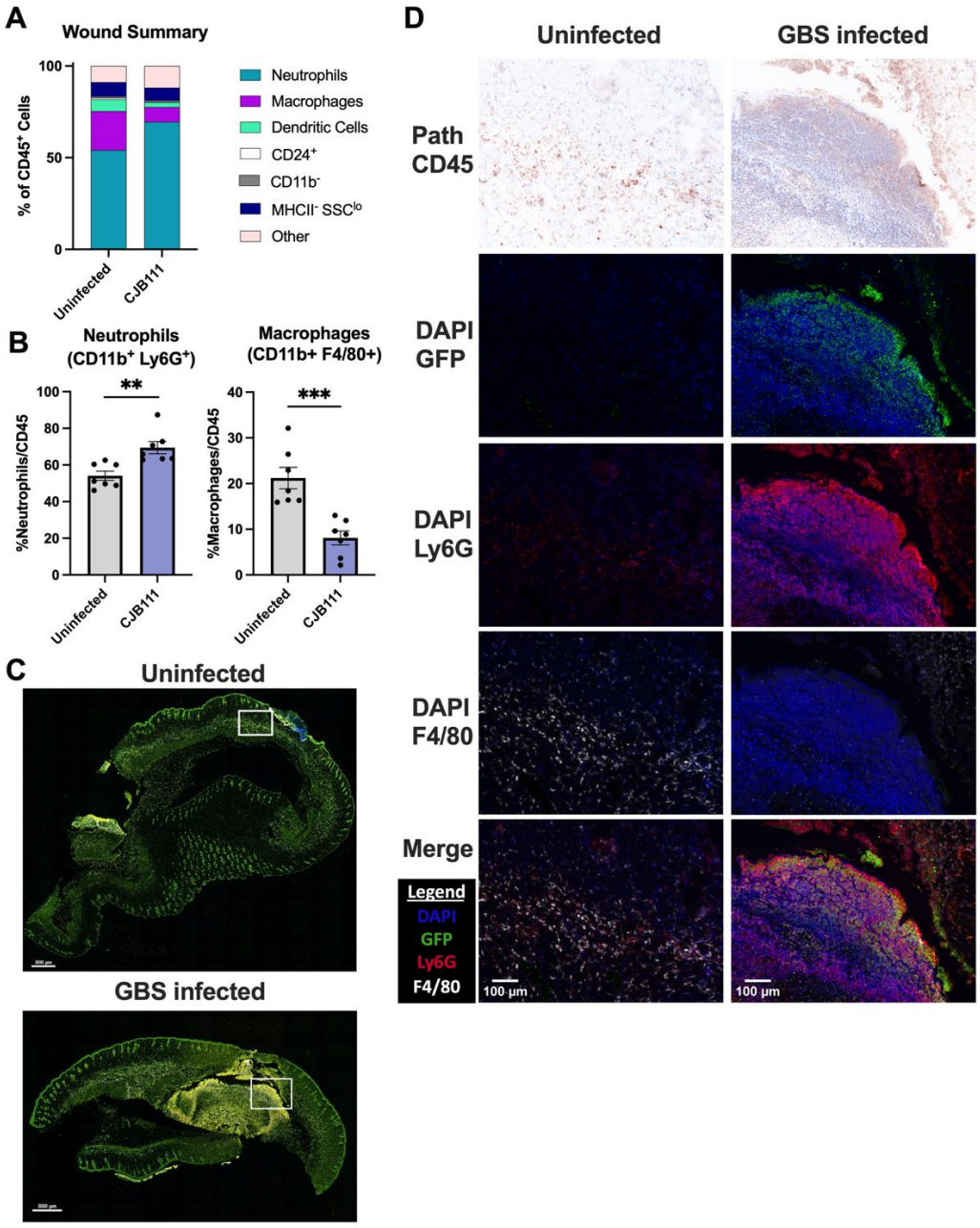


568

569 **Figure 1**. **Neutrophils are abundant in the diabetic wound during infection.** A)
570 Wound immune cell populations measured by flow cytometry. B) A significant increase of
571 neutrophils (left) and significant decrease of macrophages (right) as a percent of $CD45^+$
572 immune cells is observed in GBS infected diabetic wounds at 48 h compared to uninfected
573 diabetic wounds. C) Multispectral immunohistochemistry microscopy images of diabetic
574 wound tissues mock or GBS infected. Scale bar 800 µm. D) White boxed region of
575 interested showing CD45 pathology, GFP expressing GBS in the wound, $Ly6G^+$
576 neutrophil marker, $F4/80^+$ macrophage marker, and merged image. Scale bar 100 µm.
577 Significance determined by B) two-tailed T-Test; **p<.01; ***p<.001.

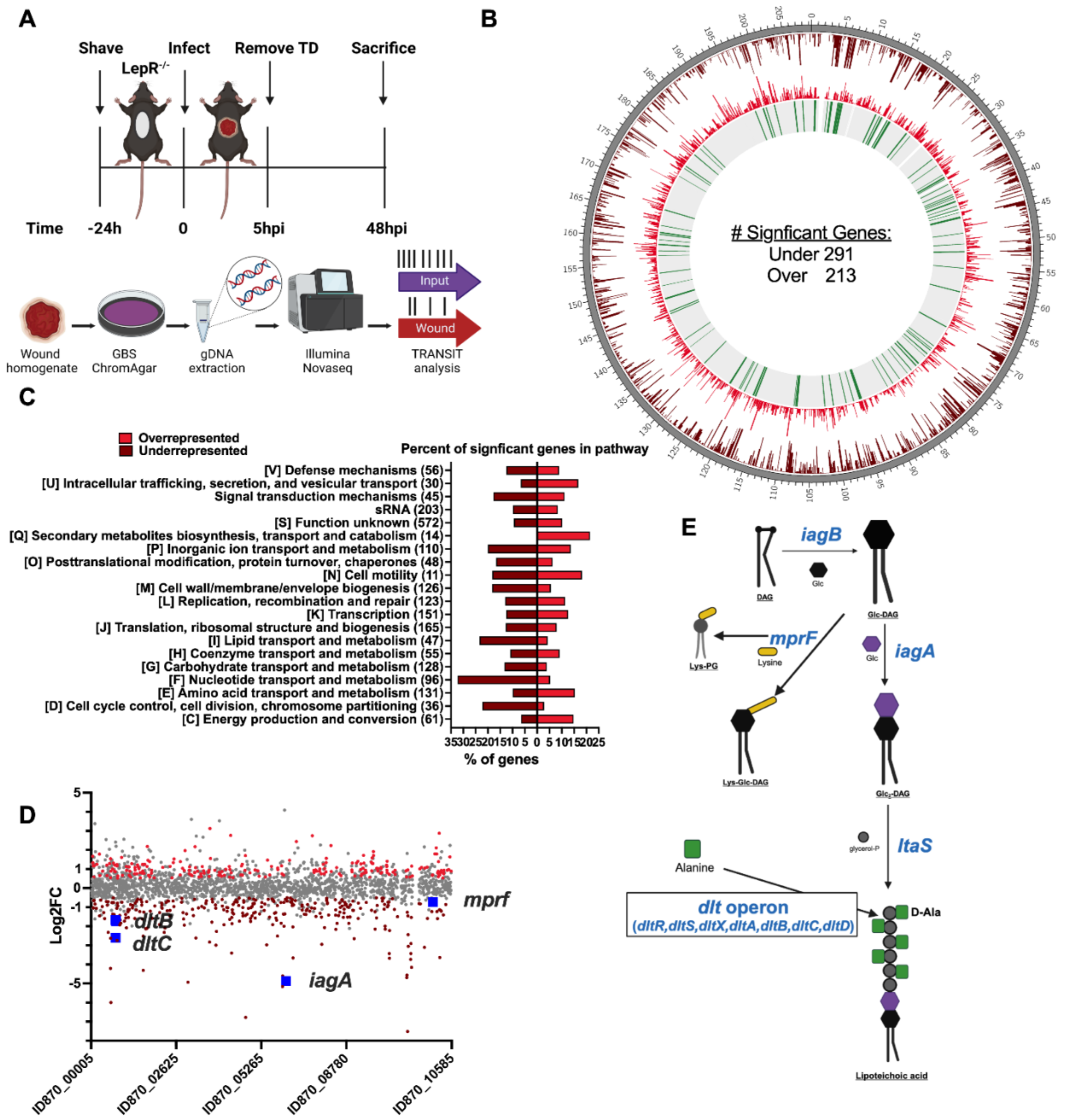


**Figure 2. Essential GBS Genes During Diabetic Wound Infection.** A) Experimental set-up for Tn-seq. B) CIRCOS plot showing from outer ringer to inner ring; dark grey, genome length in Kb; maroon, negative Log2Fold Change (L2FC); red, positive L2FC; statistically significant genes (adj. p-value ≤ 0.05) shown in green and non-significant genes in light grey. C) COG pathway analysis of percent of statistically significant genes in each COG for both over- (red) and under- (maroon) represented genes. (Numbers) indicate the total number of genes in each pathway. D) Linear plot of significantly over (red) and underrepresented (maroon) genes ordered by genomic position. E) Glycolipid biosynthesis and LTA decoration pathway in GBS.

588

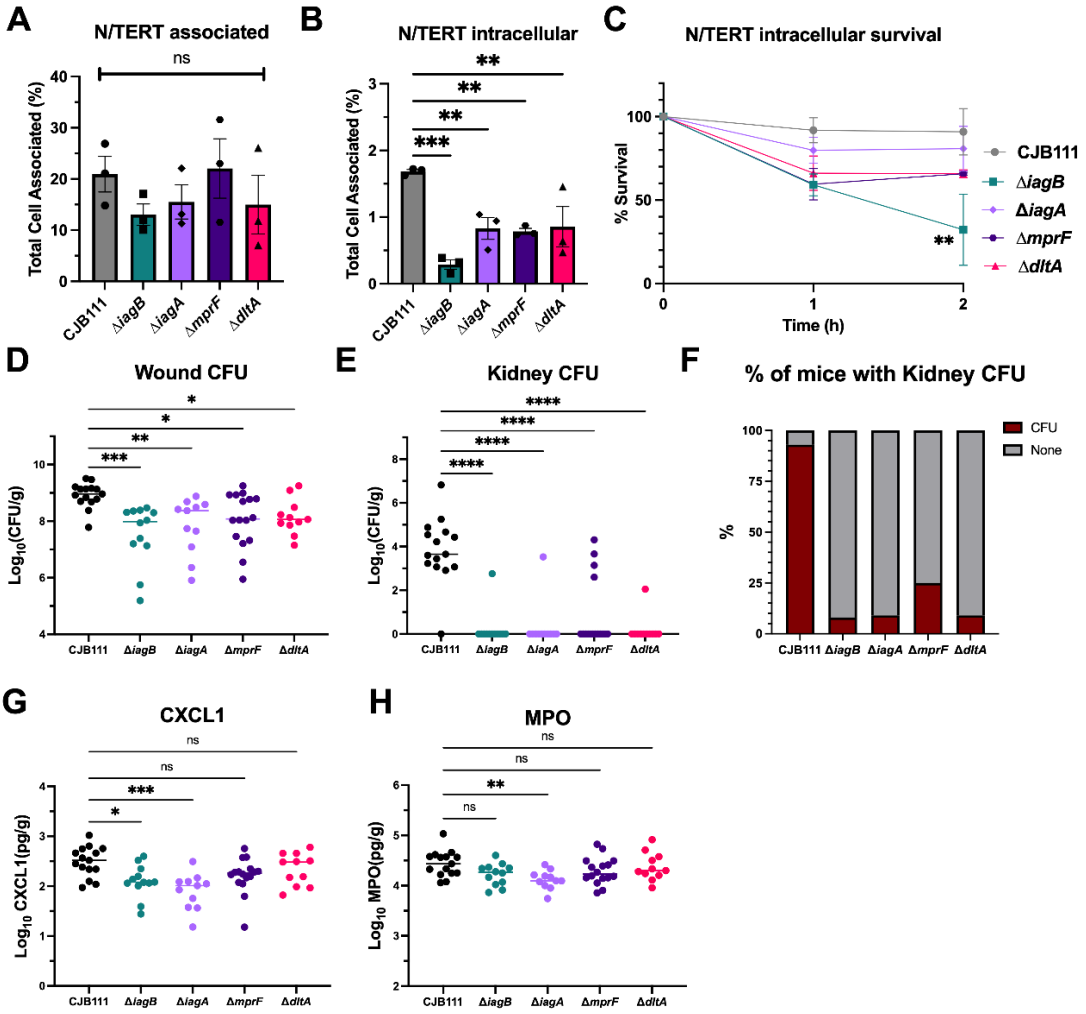


589

590 **Figure 3. Glycolipid biosynthesis enzymes and LTA alanylation are necessary for**
591 **epithelial cell invasion and survival in diabetic wound infection**. *In vitro* assays for
592 A) total cell associated (adherence) and B) intracellular GBS after 2 h infection, of GBS
593 mutants N/TERTs indicate GBS glycolipids and LTA alanylation are dispensable for
594 adhesion but are important for invasion of skin epithelial cells. C) Intracellular survival of
595 GBS mutants over 2 h indicates GBS glycolipids are important for intracellular survival.
596 Each assay was performed in biological triplicate, with three technical replicates per
597 assay. Mean and SEM indicated. Diabetic mice were inoculated with 1 x $10^7$ CFU of GBS
598 WT, Δ*iagB*, Δ*iagA*, Δ*mprF*, and Δ*dltA* isogeneic mutants and bacterial burdens were
599 assessed after 48 h in the D) wound and E) kidneys. Significantly less CFU of all four
600 mutants are recovered from the wound and kidneys of infected mice. F) % of mice in
601 each infection group with detectable CFU in kidneys. G) Chemokine CXCL-1 and H)
602 myeloperoxidase protein production measured by ELISA from wound tissues. Median
603 indicated. GBS WT; *n* = 15, Δ*iagB; n* = 12, Δ*iagA*; *n* = 11, Δ*mprF*; *n* = 16, and Δ*dltA;* n =
604 11. Significance determined by A-C) One-way ANOVA with Fisher LSD and D,E,G,H)
605 Kruskal-Wallis with Dunn's multiple comparisons test; *p<.05, **p<.01, ***p<.001,
606 ****p<.0001. ns; not significant.

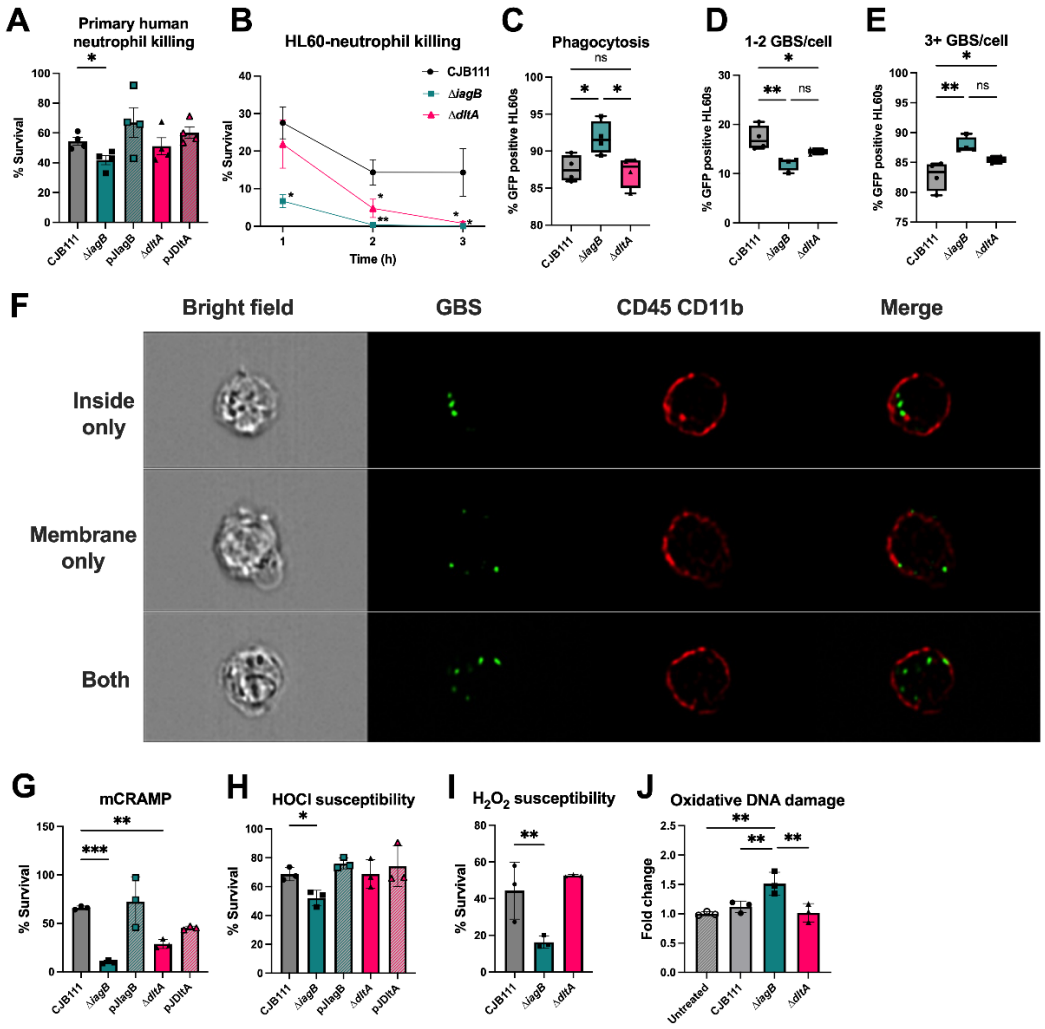


**Figure 4. GBS susceptibility to neutrophil killing factors.** A) Primary human neutrophil killing of GBS WT, GBS∆*iagB*, pJIagB, GBS∆*dltA*, and pJDltA in high glucose infected at MOI 25 for 1 h. % Survival calculated as the ratio of CFU with neutrophils versus CFU without neutrophils. B) HL60-neutrophil like cell killing of GBS WT, ∆*iagB* and ∆*dltA* at MOI 0.001 for 3 h. % Survival calculated as the ratio of CFU in normal serum versus CFU in heat-killed serum in the presence of HL60 cells. C) Phagocytosis frequency of GBS WT, GBS∆*iagB,* and GBS∆*dltA* by HL60 cells infected at MOI 8-10 measured by imaging flow cytometry indicated as percent GFP positive HL60 cells, D) 1-2 GBS per cell and E) 3 or more GBS per cell. GBS∆*iagB* is phagocytized at a higher rate than GBS WT and both GBS∆*iagB* and GBS∆*dltA* have higher number of bacteria per neutrophil compared to WT. F) Representative image of GBS WT phagocytosis in HL60 cells. G) Percent survival of GBS WT, GBS∆*iagB*, pJIagB, GBS∆*dltA*, and pJDltA to D) mouse cathelicidin mCRAMP after 30 min and H) hypochlorite (HOCl). I) Percent survival of GBS WT, GBS∆*iagB*, and GBS∆*dltA*, to 100 µg $H_2O_2$ after 1 h and J) Oxidative DNA damage caused by $H_2O_2$ measured via ELISA. A) Mean and SEM, B,G-J) Mean and SD. C-E) Min to Max. Significance determined by A) Mann-Whitney B-J) One-way ANOVA with Fishers LSD test; *p<.05, **p<.01, ***p<.001. Each assay was performed in at least biological triplicate.

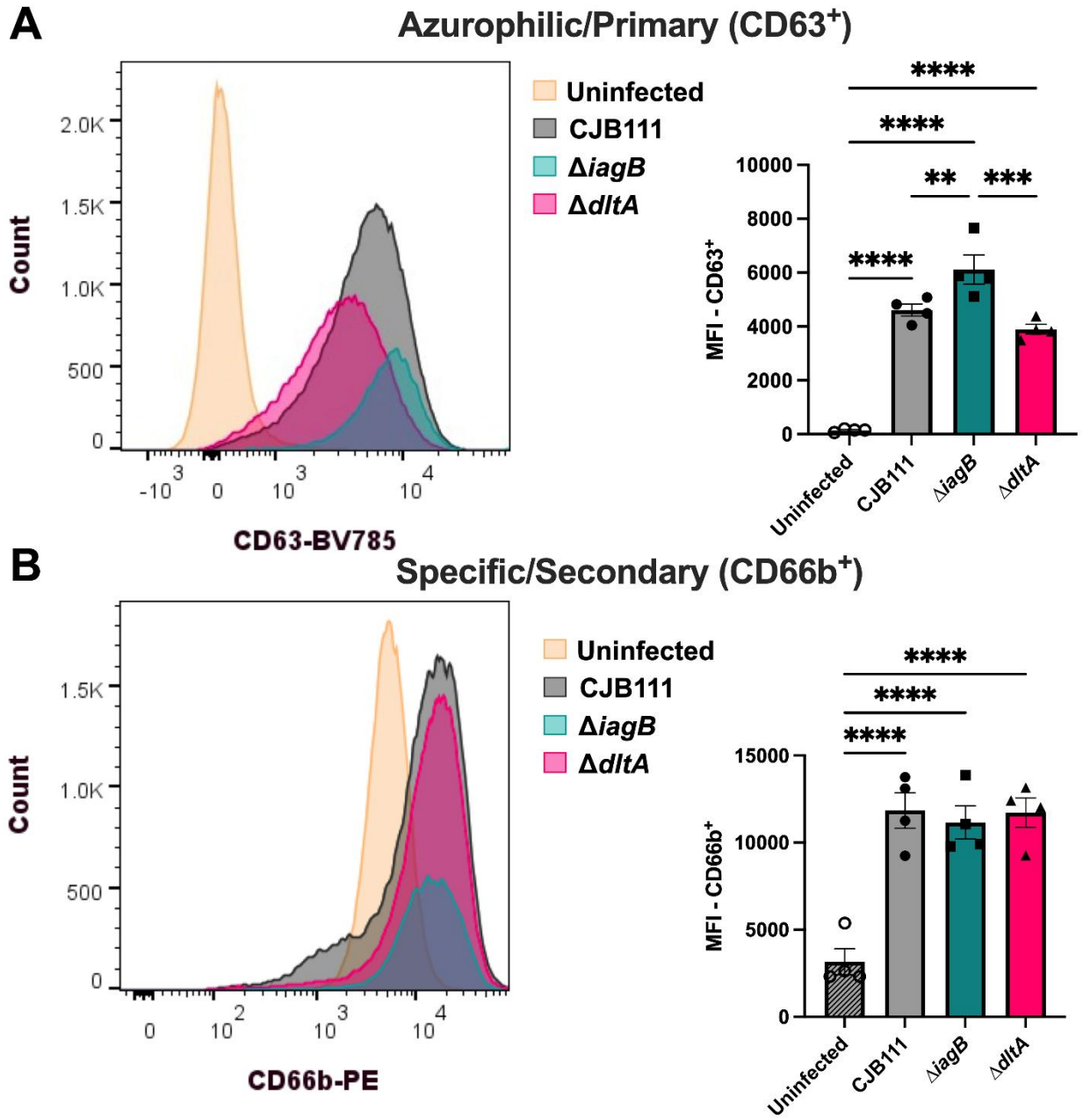


**Figure 5. GBS glycolipids and LTA alanylation is not required for degranulation in primary human neutrophils.** Neutrophil degranulation measured in primary human neutrophils conditioned in high glucose exposed to opsonized GBS by flow cytometry after 30 min. A) Azurophilic/primary ($CD63^+$) granules: left; representative histogram of counts of $CD63^+$ neutrophils and right; median fluorescent intensity (MFI) of CD63. Specific/secondary granules B) $CD66b^+$. A significant increase in both primary and secondary degranulation compared to uninfected neutrophils is observed. A-C) Mean and SEM. A-C) Significance determined by One-way ANOVA with Fisher's LSD test; *p<.05, **p<.01, ***p<.001, ****p<.0001, ns; not significant. Assay was performed in at biological quadruplicate.

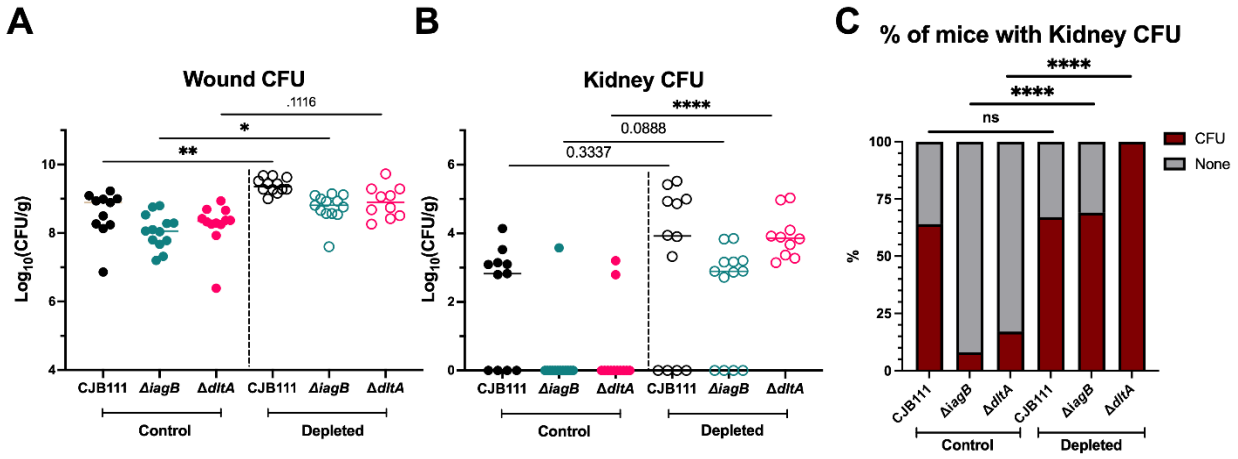


**Figure 6. Neutrophils play an important role in combating GBS in the diabetic wound.** Control (anti-IgG2a antibody, closed circles) and neutrophil depleted diabetic mice (anti-Ly6G antibody, open circles) were infected with 1 x $10^7$ GBS WT, Δ*iagB*, and Δ*dltA* and bacterial burdens were assessed at 48h in the A) wound and B) kidney. Significantly higher bacterial burdens were recovered in the wound and kidney in depleted mice compared to control mice. C) % of mice in each group with CFU in the kidney. Control: GBS WT; *n* = 11, Δ*iagB; n* = 13, and Δ*dltA;* n = 12. Depleted: GBS WT; *n* = 12, Δ*iagB; n* = 13, and Δ*dltA;* n = 10. Significance determined by A,B) Kruskal-Wallis test with Dunn's multiple comparisons, C) Fishers exact test; *p<.05, **p<.01, ****p<.0001.

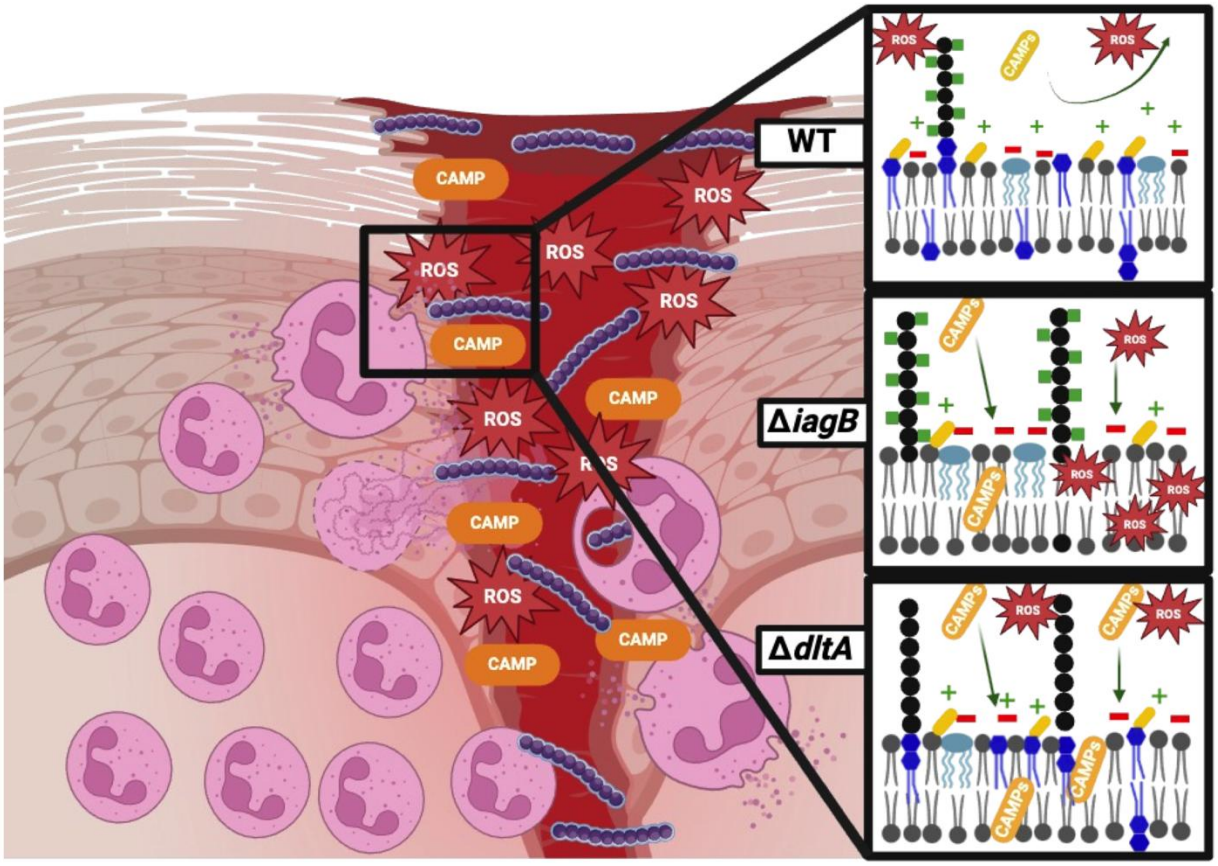


**Figure 7. GBS glycolipids and LTA alanylation promote diabetic wound colonization.** GBS infects the diabetic wound where it encounters a large population of neutrophils in the wound. Neutrophils are recruited to the wound to control the infection. The diabetic wound is rich in multiple antimicrobial molecules such as cationic antimicrobial peptides (CAMP) and reactive oxygen species (ROS). GBS∆*dltA* is unable to modify lipoteichoic acid (LTA) and is more susceptible to both neutrophil killing and CAMPs compared to GBS WT, whereas *GBS∆iagB* lacking all glycolipids is hypersusceptible to neutrophil killing, CAMPs and ROS attack.

658 **REFERENCES**


659 1. Sun, H., Saeedi, P., Karuranga, S., Pinkepank, M., Ogurtsova, K., Duncan, B.B.,
660 Stein, C., Basit, A., Chan, J.C.N., Mbanya, J.C., et al. (2022). IDF Diabetes Atlas:
661 Global, regional and country-level diabetes prevalence estimates for 2021 and
662 projections for 2045. Diabetes Res Clin Pract *183*, 109119.
663 https://doi.org/10.1016/j.diabres.2021.109119.

664 2. Hingorani, A., Lamuraglia, G.M., Henke, P., Meissner, M.H., Loretz, L., Zinszer,
665 K.M., Driver, V.R., Frykberg, R., Carman, T.L., Marston, W., et al. (2016). The
666 management of diabetic foot: A clinical practice guideline by the Society for
667 Vascular Surgery in collaboration with the American Podiatric Medical Association
668 and the Society for Vascular Medicine. J Vasc Surg *63*, 3S-21S.
669 https://doi.org/10.1016/j.jvs.2015.10.003.

670 3. Uccioli, L., Izzo, V., Meloni, M., Vainieri, E., Ruotolo, V., and Giurato, L. (2015).
671 Non-healing foot ulcers in diabetic patients: general and local interfering
672 conditions and management options with advanced wound dressings. J Wound
673 Care *24*, 35–42. https://doi.org/10.12968/jowc.2015.24.Sup4b.35.

674 4. Loots, M.A.M., Lamme, E.N., Zeegelaar, J., Mekkes, J.R., Bos, J.D., and
675 Middelkoop, E. (1998). Differences in cellular infiltrate and extracellular matrix of
676 chronic diabetic and venous ulcers versus acute wounds. Journal of Investigative
677 Dermatology *111*, 850–857. https://doi.org/10.1046/j.1523-1747.1998.00381.x.

678 5. Eming, S.A., Krieg, T., and Davidson, J.M. (2007). Inflammation in wound repair:
679 Molecular and cellular mechanisms. Journal of Investigative Dermatology *127*,
680 514–525. https://doi.org/10.1038/sj.jid.5700701.

681 6. Grice, E.A., and Segre, J.A. (2012). Interaction of the microbiome with the innate
682 immune response in chronic wounds. Adv Exp Med Biol *946*, 55–68.
683 https://doi.org/10.1007/978-1-4614-0106-3_4.

684 7. Singer, A.J., and Clark, R.A.F. (1999). Cutaneous Wound Healing. New England
685 Journal of Medicine *341*, 738–746.
686 https://doi.org/10.1056/NEJM199909023411006.

687 8. Kalan, L.R., Meisel, J.S., Loesche, M.A., Horwinski, J., Soaita, I., Chen, X.,
688 Uberoi, A., Gardner, S.E., and Grice, E.A. (2019). Strain- and Species-Level
689 Variation in the Microbiome of Diabetic Wounds Is Associated with Clinical
690 Outcomes and Therapeutic Efficacy. Cell Host Microbe *25*, 641-655.e5.
691 https://doi.org/10.1016/j.chom.2019.03.006.

692 9. Keogh, R.A., Huyvaert, S., Moore, G.D., Horswill, A.R., and Doran, K.S. (2024).
693 Virulence characteristics of Gram-positive bacteria isolated from diabetic foot
694 ulcers. FEMS Microbes *5*, 1–10. https://doi.org/10.1093/femsmc/xtae013.

695 10. Rahim, K., Saleha, S., Zhu, X., Huo, L., Basit, A., and Franco, O.L. (2017).
696 Bacterial Contribution in Chronicity of Wounds. Microb Ecol *73*, 710–721.
697 https://doi.org/10.1007/s00248-016-0867-9.

698 11. Gardner, S.E., Hillis, S.L., Heilmann, K., Segre, J.A., and Grice, E.A. (2013). The
699 neuropathic diabetic foot ulcer microbiome is associated with clinical factors.
700 Diabetes *62*, 923–930. https://doi.org/10.2337/db12-0771.

701 12. Jeffcoate, W.J., and Harding, K.G. (2003). Diabetic foot ulcers. Lancet *361*, 1545–
702 1551. https://doi.org/10.1016/S0140-6736(03)13169-8.

703 13. Jeffcoate, W.J., Price, P., and Harding, K.G. (2004). Wound healing and
704 treatments for people with diabetic foot ulcer. Diabetes Metab Res Rev *20*, 78–89.
705 https://doi.org/10.1002/dmrr.476.

706 14. Perim, M.C., Borges, J. da C., Celeste, S.R.C., Orsolin, E. de F., Mendes, R.R.,
707 Mendes, G.O., Ferreira, R.L., Carreiro, S.C., and Da Silva Pranchevicius, M.C.
708 (2015). Aerobic bacterial profile and antibiotic resistance in patients with diabetic
709 foot infections. Rev Soc Bras Med Trop *48*, 546–554.
710 https://doi.org/10.1590/0037-8682-0146-2015.

711 15. Wolcott, R.D., Hanson, J.D., Rees, E.J., Koenig, L.D., Phillips, C.D., Wolcott,
712 R.A., Cox, S.B., and White, J.S. (2016). Analysis of the chronic wound microbiota
713 of 2,963 patients by 16S rDNA pyrosequencing. Wound Repair and Regeneration
714 *24*, 163–174. https://doi.org/10.1111/wrr.12370.

715 16. ALbeloushi, A., Elbehiry, A., Marzouk, E., Zahran, R., and Edrees, H. (2019).
716 Highlight on multidrug resistance of enterococcus faecalis recovered from diabetic
717 foot patients. J Pure Appl Microbiol *13*, 481–489.
718 https://doi.org/10.22207/JPAM.13.1.54.

719 17. Kalan, L.R., and Brennan, M.B. (2019). The role of the microbiome in nonhealing
720 diabetic wounds. Ann N Y Acad Sci *1435*, 79–92.
721 https://doi.org/10.1111/nyas.13926.

722 18. Shook, J.C., Genito, C.J., Darwitz, B.P., Tyson, K.J., Velez, A.Z., Bridwell, S.K.,
723 Parsons, J.B., Rowe, S.E., Marshall, C.W., Conlon, B.P., et al. (2025). Diabetes
724 potentiates the emergence and expansion of antibiotic resistance. *1591*.
725 https://doi.org/10.1126/sciadv.ads1591.

726 19. James, G.A., Swogger, E., Wolcott, R., Pulcini, E.D., Secor, P., Sestrich, J.,
727 Costerton, J.W., and Stewart, P.S. (2008). Biofilms in chronic wounds. Wound
728 Repair and Regeneration *16*, 37–44. https://doi.org/10.1111/j.1524-
729 475X.2007.00321.x.

730 20. Watters, C., Everett, J.A., Haley, C., Clinton, A., and Rumbaugh, K.P. (2014).
731 Insulin treatment modulates the host immune system to enhance Pseudomonas

732 aeruginosa wound biofilms. Infect Immun *82*, 92–100.
733 https://doi.org/10.1128/IAI.00651-13.

734 21. Ch'ng, J.-H., Muthu, M., Chong, K.K.L., Wong, J.J., Tan, C.A.Z., Koh, Z.J.S.,
735 Lopez, D., Matysik, A., Nair, Z.J., Barkham, T., et al. (2022). Heme cross-feeding
736 can augment Staphylococcus aureus and Enterococcus faecalis dual species
737 biofilms. ISME J. https://doi.org/10.1038/s41396-022-01248-1.

738 22. Cowley, E.S., Chaves, I.Z., Osman, F., Suen, G., Anantharaman, K., and
739 Hryckowian, A.J. (2023). Determinants of Gastrointestinal Group B Streptococcus
740 Carriage in Adults. Preprint, https://doi.org/10.1101/2023.08.17.553755
741 https://doi.org/10.1101/2023.08.17.553755.

742 23. Doran, K.S., and Nizet, V. (2004). Molecular pathogenesis of neonatal group B
743 streptococcal infection: No longer in its infancy. Mol Microbiol *54*, 23–31.
744 https://doi.org/10.1111/j.1365-2958.2004.04266.x.

745 24. Wilkinson, H.W. (1978). Group B Streptococcal Infection in Humans. Annu Rev
746 Microbiol *32*, 41–57. https://doi.org/10.1146/annurev.mi.32.100178.000353.

747 25. Kline, K.A., and Lewis, A.L. (2016). Gram-positive uropathogens, polymicrobial
748 urinary tract infection, and the emerging microbiota of the urinary tract. Urinary
749 Tract Infections: Molecular Pathogenesis and Clinical Management, 459–502.
750 https://doi.org/10.1128/9781555817404.ch19.

751 26. Romero, R., Dey, S.K., and Fisher, S.J. (2014). Preterm labor: one syndrome,
752 many causes. Science *345*, 760–765. https://doi.org/10.1126/science.1251816.

753 27. Vornhagen, J., Armistead, B., Santana-Ufret, V., Gendrin, C., Merillat, S.,
754 Coleman, M., Quach, P., Boldenow, E., Alishetti, V., Leonhard-Melief, C., et al.
755 (2018). Group B streptococcus exploits vaginal epithelial exfoliation for ascending
756 infection. Journal of Clinical Investigation *128*, 1985–1999.
757 https://doi.org/10.1172/JCI97043.

758 28. Wang, H., Li, N., Chivese, T., Werfalli, M., Sun, H., Yuen, L., Hoegfeldt, C.A.,
759 Elise Powe, C., Immanuel, J., Karuranga, S., et al. (2022). IDF Diabetes Atlas:
760 Estimation of Global and Regional Gestational Diabetes Mellitus Prevalence for
761 2021 by International Association of Diabetes in Pregnancy Study Group's
762 Criteria. Diabetes Res Clin Pract *183*, 109050.
763 https://doi.org/10.1016/j.diabres.2021.109050.

764 29. Mercado-Evans, V., Zulk, J.J., Hameed, Z.A., and Patras, K.A. (2024).
765 Gestational diabetes as a risk factor for GBS maternal rectovaginal colonization: a
766 systematic review and meta-analysis. BMC Pregnancy Childbirth *24*, 1–16.
767 https://doi.org/10.1186/s12884-024-06694-7.

768 30. Zhou, Y., Wang, L.-Q., Yan, Q., Lee, C.-C., Hsu, M.-H., Liao, W.-T., Zhang, L.,
769 and Chiu, C.-H. (2022). Genomic Analysis of Group B Streptococcus from

770 Neonatal Sepsis Reveals Clonal CC17 Expansion and Virulence- and Resistance-
771 Associated Traits After Intrapartum Antibiotic Prophylaxis. Clinical Infectious
772 Diseases *75*, 2153–2160. https://doi.org/10.1093/cid/ciac331.

773 31. Uggen, E., Olaisen, C., Valsø, R., Gunnar, L., Simonsen, S., Magne, R., Jensen,
774 B., Width, F., Bjørn, G., Åsvold, O., et al. (2024). Incidence of invasive infections
775 with Group B streptococcus in adults in Norway 1996 – 2019 : a nationwide
776 registry - based case – control study. Infection. https://doi.org/10.1007/s15010-
777 024-02210-3.

778 32. Edwards, M.S., and Baker, C.J. (2005). Group B streptococcal infections in
779 elderly adults. Clinical Infectious Diseases *41*, 839–847.
780 https://doi.org/10.1086/432804.

781 33. Melin, P. (2011). Neonatal group B streptococcal disease: from pathogenesis to
782 preventive strategies. Clinical Microbiology and Infection *17*, 1294–1303.
783 https://doi.org/10.1111/j.1469-0691.2011.03576.x.

784 34. Nguyen, L.M., Omage, J.I., Noble, K., McNew, K.L., Moore, D.J., Aronoff, D.M.,
785 and Doster, R.S. (2021). Group B streptococcal infection of the genitourinary tract
786 in pregnant and non-pregnant patients with diabetes mellitus: An
787 immunocompromised host or something more? Preprint,
788 https://doi.org/10.1111/aji.13501 https://doi.org/10.1111/aji.13501.

789 35. NS Raja (2007). Microbiology of diabetic foot infections in a teaching hospital in
790 Malaysia: a retrospective study of 194 cases. Journal of microbiology immunology
791 and infection *40*, 39.

792 36. Heravi, F.S., Zakrzewski, M., Vickery, K., Malone, M., and Hu, H. (2020).
793 Metatranscriptomic Analysis Reveals Active Bacterial Communities in Diabetic
794 Foot Infections. Front Microbiol *11*, 1–10.
795 https://doi.org/10.3389/fmicb.2020.01688.

796 37. Citron, D.M., Goldstein, E.J.C., Merriam, C.V., Lipsky, B.A., and Abramson, M.A.
797 (2007). Bacteriology of moderate-to-severe diabetic foot infections and in vitro
798 activity of antimicrobial agents. J Clin Microbiol *45*, 2819–2828.
799 https://doi.org/10.1128/JCM.00551-07.

800 38. Wang, Y., Zhang, H., Ma, G., Tian, Z., and Wang, B. (2022). The contribution of
801 intestinal Streptococcus to the pathogenesis of diabetic foot ulcers: An analysis
802 based on 16S rRNA sequencing. Int Wound J *19*, 1658–1668.
803 https://doi.org/10.1111/iwj.13766.

804 39. Blancas, D., Santin, M., Olmo, M., Alcaide, F., Carratala, J., and Gudiol, F.
805 (2004). Group B Streptococcal Disease in Nonpregnant Adults: Incidence, Clinical
806 Characteristics, and Outcome. European Journal of Clinical Microbiology &
807 Infectious Diseases *23*, 168–173. https://doi.org/10.1007/s10096-003-1098-9.

808 40. Loesche, M., Gardner, S.E., Kalan, L., Horwinski, J., Zheng, Q., Hodkinson, B.P.,
809 Tyldsley, A.S., Franciscus, C.L., Hillis, S.L., Mehta, S., et al. (2017). Temporal
810 Stability in Chronic Wound Microbiota Is Associated With Poor Healing. Journal of
811 Investigative Dermatology *137*, 237–244. https://doi.org/10.1016/j.jid.2016.08.009.

812 41. Keogh, R.A., Haeberle, A.L., Langouët-Astrié, C.J., Kavanaugh, J.S., Schmidt,
813 E.P., Moore, G.D., Horswill, A.R., and Doran, K.S. (2022). Group B Streptococcus
814 adaptation promotes survival in a hyperinflammatory diabetic wound environment.
815 Sci Adv *8*. https://doi.org/10.1126/sciadv.add3221.

816 42. Joyce, L.R., and Doran, K.S. (2023). Gram-positive bacterial membrane lipids at
817 the host-pathogen interface. PLoS Pathog *19*, 1–7.
818 https://doi.org/10.1371/journal.ppat.1011026.

819 43. Joyce, L.R., Kim, S., Spencer, B.L., Christensen, P.M., Palmer, K.L., Guan, Z.,
820 Siegenthaler, J.A., and Doran, K.S. (2024). Streptococcus agalactiae glycolipids
821 promote virulence by thwarting immune cell clearance. Sci Adv *10*, 1–15.
822 https://doi.org/10.1126/sciadv.adn7848.

823 44. Joyce, L.R., Manzer, H.S., Mendonça, J. da C., Villarreal, R., Nagao, P.E., Doran,
824 K.S., Palmer, K.L., and Guan, Z. (2022). Identification of a novel cationic
825 glycolipid in Streptococcus agalactiae that contributes to brain entry and
826 meningitis. PLoS Biol *20*, 1–15. https://doi.org/10.1371/journal.pbio.3001555.

827 45. Doran, K.S., Engelson, E.J., Khosravi, A., Maisey, H.C., Fedtke, I., Equils, O.,
828 Michelsen, K.S., Arditi, M., Peschel, A., and Nizet, V. (2005). Blood-brain barrier
829 invasion by group B Streptococcus depends upon proper cell-surface anchoring
830 of lipoteichoic acid. Journal of Clinical Investigation *115*, 2499–2507.
831 https://doi.org/10.1172/JCI23829.

832 46. Shrestha, S., Lee, Y.-B., Lee, H., Choi, Y.-K., Park, B.-Y., Kim, M.-J., Youn, Y.-J.,
833 Kim, S.-H., Jung, S.-J., Song, D.-K., et al. (2024). Diabetes Primes Neutrophils for
834 Neutrophil Extracellular Trap Formation through Trained Immunity. Research *7*,
835 1–14. https://doi.org/10.34133/research.0365.

836 47. Spencer, B.L., Nguyen, D.T., Marroquin, S.M., Gapin, L., O'Brien, R.L., and
837 Doran, K.S. (2025). Characterization of the Cellular Immune Response to Group
838 B Streptococcal Vaginal Colonization. bioRxiv.
839 https://doi.org/10.1101/2025.01.29.635275.

840 48. Burcham, L.R., Akbari, M.S., Alhajjar, N., Keogh, R.A., Radin, J.N., Kehl-Fie, T.E.,
841 Belew, A.T., El-Sayed, N.M., McIver, K.S., and Doran, K.S. (2022). Genomic
842 Analyses Identify Manganese Homeostasis as a Driver of Group B Streptococcal
843 Vaginal Colonization. mBio *13*. https://doi.org/10.1128/mbio.00985-22.

844 49. Burcham, L.R., Le Breton, Y., Radin, J.N., Spencer, B.L., Deng, L., Hiron, A.,
845 Ransom, M.R., Mendonça, J. da C., Belew, A.T., El-Sayed, N.M., et al. (2020).

846 Identification of zinc-dependent mechanisms used by Group B Streptococcus to
847 overcome calprotectin-mediated stress. mBio *11*, 1–18.
848 https://doi.org/10.1101/2020.08.14.252064.

849 50. Akbari, M.S., Joyce, L.R., Spencer, B.L., Brady, A., McIver, K.S., and Doran, K.S.
850 (2025). Identification of glyoxalase A in group B Streptococcus and its contribution
851 to methylglyoxal tolerance and virulence. Infect Immun *0*, e0054024.
852 https://doi.org/10.1128/iai.00540-24.

853 51. Spencer, B.L., Chatterjee, A., Duerkop, B.A., Baker, C.J., and Doran, K.S. (2021).
854 Complete Genome Sequence of Neonatal Clinical Group B Streptococcal Isolate
855 CJB111. Microbiol Resour Announc *10*, 14–16.
856 https://doi.org/10.1128/mra.01268-20.

857 52. Flores, A.R., Galloway-Peña, J., Sahasrabhojane, P., Saldaña, M., Yao, H., Su,
858 X., Ajami, N.J., Holder, M.E., Petrosino, J.F., Thompson, E., et al. (2015).
859 Sequence type 1 group B Streptococcus, an emerging cause of invasive disease
860 in adults, evolves by small genetic changes. Proc Natl Acad Sci U S A *112*, 6431–
861 6436. https://doi.org/10.1073/pnas.1504725112.

862 53. Pritzlaff, C.A., Chang, J.C.W., Kuo, S.P., Tamura, G.S., Rubens, C.E., and Nizet,
863 V. (2001). Genetic basis for the β-haemolytic/cytolytic activity of group B
864 streptococcus. Mol Microbiol *39*, 236–248. https://doi.org/10.1046/j.1365-
865 2958.2001.02211.x.

866 54. Armistead, B., Oler, E., Waldorf, K.A., Rajagopal, L., and Disease, I. (2019). The
867 double life of Group B Streptococcus: Asymptomatic colonizer and potent
868 pathogen. J Mol Biol *431*, 2914–2931.
869 https://doi.org/10.1016/j.jmb.2019.01.035.The.

870 55. Rajagopal, L. (2009). Understanding the regulation of Group B Streptococcal
871 virulence factors. Future Microbiol *4*, 201–221.
872 https://doi.org/10.2217/17460913.4.2.201.

873 56. Kolar, S.L., Kyme, P., Tseng, C.W., Soliman, A., Kaplan, A., Liang, J., Nizet, V.,
874 Jiang, D., Murali, R., Arditi, M., et al. (2015). Group B Streptococcus Evades Host
875 Immunity by Degrading Hyaluronan. Cell Host Microbe *18*, 694–704.
876 https://doi.org/10.1016/j.chom.2015.11.001.

877 57. Dubbs, J.M., and Mongkolsuk, S. (2012). Peroxide-sensing transcriptional
878 regulators in bacteria. J Bacteriol *194*, 5495–5503.
879 https://doi.org/10.1128/JB.00304-12.

880 58. Lalioui, L., Pellegrini, E., Dramsi, S., Baptista, M., Bourgeois, N., Doucet-
881 Populaire, F., Rusniok, C., Zouine, M., Glaser, P., Kunst, F., et al. (2005). The
882 SrtA sortase of Streptococcus agalactiae is required for cell wall anchoring of
883 proteins containing the LPXTG motif, for adhesion to epithelial cells, and for

884 colonization of the mouse intestine. Infect Immun *73*, 3342–3350.
885 https://doi.org/10.1128/IAI.73.6.3342-3350.2005.

886 59. Spencer, B.L., Job, A.M., Robertson, C.M., Hameed, Z.A., Serchejian, C., Wiafe-
887 Kwakye, C.S., Mendonça, J.C., Apolonio, M.A., Nagao, P.E., Neely, M.N., et al.
888 (2023). Heterogeneity of the group B streptococcal type VII secretion system and
889 influence on colonization of the female genital tract
890 https://doi.org/10.1111/mmi.15115.

891 60. Faralla, C., Metruccio, M.M., De Chiara, M., Mu, R., Patras, K.A., Muzzi, A.,
892 Grandi, G., Margarit, I., Doran, K.S., and Janulczyk, R. (2014). Analysis of two-
893 component systems in group B streptococcus shows that RgfAC and the novel
894 FspSR modulate virulence and bacterial fitness. mBio *5*, 1–12.
895 https://doi.org/10.1128/mBio.00870-14.

896 61. Thomas, L., and Cook, L. (2020). Two-component signal transduction systems in
897 the human pathogen streptococcus agalactiae. Infect Immun *88*, 1–16.
898 https://doi.org/10.1128/IAI.00931-19.

899 62. Quach, D., Van Sorge, N.M., Kristian, S.A., Bryan, J.D., Shelver, D.W., and
900 Doran, K.S. (2009). The ciar response regulator in group b streptococcus
901 promotes intracellular survival and resistance to innate immune defenses. J
902 Bacteriol *191*, 2023–2032. https://doi.org/10.1128/JB.01216-08.

903 63. Spencer, B.L., Deng, L., Patras, K.A., Burcham, Z.M., Sanches, G.F., Nagao,
904 P.E., and Doran, K.S. (2019). Cas9 contributes to group b streptococcal
905 colonization and disease. Front Microbiol *10*, 1–15.
906 https://doi.org/10.3389/fmicb.2019.01930.

907 64. Poyart, C., Pellegrini, E., Marceau, M., Baptista, M., Jaubert, F., Lamy, M.C., and
908 Trieu-Cuot, P. (2003). Attenuated virulence of Streptococcus agalactiae deficient
909 in D-alanyl-lipoteichoic acid is due to an increased susceptibility to defensins and
910 phagocytic cells. Mol Microbiol *49*, 1615–1625. https://doi.org/10.1046/j.1365-
911 2958.2003.03655.x.

912 65. Poyart, C., Lamy, M.C., Boumaila, C., Fiedler, F., and Trieu-Cuot, P. (2001).
913 Regulation of D-alanyl-lipoteichoic acid biosynthesis in Streptococcus agalactiae
914 involves a novel two-component regulatory system. J Bacteriol *183*, 6324–6334.
915 https://doi.org/10.1128/JB.183.21.6324-6334.2001.

916 66. Noble, K., Lu, J., Guevara, M.A., Doster, R.S., Chambers, S.A., Rogers, L.M.,
917 Moore, R.E., Spicer, S.K., Eastman, A.J., Francis, J.D., et al. (2021). Group B
918 Streptococcus cpsE Is Required for Serotype V Capsule Production and Aids in
919 Biofilm Formation and Ascending Infection of the Reproductive Tract during
920 Pregnancy. ACS Infect Dis *7*, 2686–2696.
921 https://doi.org/10.1021/acsinfecdis.1c00182.

922 67. Carlin, A.F., Chang, Y.C., Areschoug, T., Lindahl, G., Hurtado-Ziola, N., King,
923 C.C., Varki, A., and Nizet, V. (2009). Group B Streptococcus suppression of
924 phagocyte functions by protein-mediated engagement of human Siglec-5. Journal
925 of Experimental Medicine *206*, 1691–1699. https://doi.org/10.1084/jem.20090691.

926 68. Uchiyama, S., Sun, J., Fukahori, K., Ando, N., Wu, M., Schwarz, F., Siddiqui,
927 S.S., Varki, A., Marth, J.D., and Nizet, V. (2019). Dual actions of group B
928 Streptococcus capsular sialic acid provide resistance to platelet-mediated
929 antimicrobial killing. Proc Natl Acad Sci U S A *116*, 7465–7470.
930 https://doi.org/10.1073/pnas.1815572116.

931 69. Rajagopal, L., Vo, A., Silvestroni, A., and Rubens, C.E. (2005). Regulation of
932 purine biosynthesis by a eukaryotic-type kinase in Streptococcus agalactiae. Mol
933 Microbiol *56*, 1329–1346. https://doi.org/10.1111/j.1365-2958.2005.04620.x.

934 70. Tamura, G.S., Nittayajarn, A., and Schoentag, D.L. (2002). A glutamine transport
935 gene, glnQ, is required for fibronectin adherence and virulence of group B
936 streptococci. Infect Immun *70*, 2877–2885. https://doi.org/10.1128/IAI.70.6.2877-
937 2885.2002.

938 71. Ipe, D.S., Sullivan, M.J., Goh, K.G.K., Hashimi, S.M., Munn, A.L., and Ulett, G.C.
939 (2021). Conserved bacterial de novo guanine biosynthesis pathway enables
940 microbial survival and colonization in the environmental niche of the urinary tract.
941 ISME Journal *15*, 2158–2162. https://doi.org/10.1038/s41396-021-00934-w.

942 72. Joyce, L.R., Guan, Z., and Palmer, K.L. (2021). Streptococcus pneumoniae, s.
943 Pyogenes and s. agalactiae membrane phospholipid remodelling in response to
944 human serum. Microbiology (United Kingdom) *167*.
945 https://doi.org/10.1099/mic.0.001048.

946 73. Eckert, R.L., and Rorke, E.A. (1989). Molecular biology of keratinocyte
947 differentiation. Environ Health Perspect *80*, 109–116.
948 https://doi.org/10.1289/ehp.8980109.

949 74. Smits, J.P.H., Niehues, H., Rikken, G., Van Vlijmen-Willems, I.M.J.J., Van De
950 Zande, G.W.H.J.F., Zeeuwen, P.L.J.M., Schalkwijk, J., and Van Den Bogaard,
951 E.H. (2017). Immortalized N/TERT keratinocytes as an alternative cell source in
952 3D human epidermal models. Sci Rep *7*, 1–14. https://doi.org/10.1038/s41598-
953 017-12041-y.

954 75. Patras, K.A., Wang, N.Y., Fletcher, E.M., Cavaco, C.K., Jimenez, A., Garg, M.,
955 Fierer, J., Sheen, T.R., Rajagopal, L., and Doran, K.S. (2013). Group B
956 Streptococcus CovR regulation modulates host immune signalling pathways to
957 promote vaginal colonization. Cell Microbiol *15*, 1154–1167.
958 https://doi.org/10.1111/cmi.12105.

959 76. Saar-Dover, R., Bitler, A., Nezer, R., Shmuel-Galia, L., Firon, A., Shimoni, E.,
960 Trieu-Cuot, P., and Shai, Y. (2012). D-Alanylation of Lipoteichoic Acids Confers
961 Resistance to Cationic Peptides in Group B Streptococcus by Increasing the Cell
962 Wall Density. PLoS Pathog *8*. https://doi.org/10.1371/journal.ppat.1002891.

963 77. Akbari, M.S., Keogh, R.A., Radin, J.N., Sanchez-Rosario, Y., Johnson, M.D.L.,
964 Horswill, A.R., Kehl-Fie, T.E., Burcham, L.R., and Doran, K.S. (2023). The impact
965 of nutritional immunity on Group B streptococcal pathogenesis during wound
966 infection. mBio *0*. https://doi.org/10.1128/mbio.00304-23.

967 78. Amulic, B., Cazalet, C., Hayes, G.L., Metzler, K.D., and Zychlinsky, A. (2012).
968 Neutrophil function: From mechanisms to disease. Annu Rev Immunol *30*, 459–
969 489. https://doi.org/10.1146/annurev-immunol-020711-074942.

970 79. Xu, X., and Håkansson, L. (2002). Degranulation of primary and secondary
971 granules in adherent human neutrophils. Scand J Immunol *55*, 178–188.
972 https://doi.org/10.1046/j.1365-3083.2002.01041.x.

973 80. Niyonsaba, F., Madera, L., Afacan, N., Okumura, K., Ogawa, H., and Hancock,
974 R.E.W. (2013). The innate defense regulator peptides IDR-HH2, IDR-1002, and
975 IDR-1018 modulate human neutrophil functions. J Leukoc Biol *94*, 159–170.
976 https://doi.org/10.1189/jlb.1012497.

977 81. Zanetti, M., Gennaro, R., and Romeo, D. (1995). Cathelicidins: a novel protein
978 family with a common proregion and a variable C-terminal antimicrobial domain.
979 FEBS Lett *374*, 1–5. https://doi.org/10.1016/0014-5793(95)01050-O.

980 82. Lee, T.H., Hofferek, V., Separovic, F., Reid, G.E., and Aguilar, M.I. (2019). The
981 role of bacterial lipid diversity and membrane properties in modulating
982 antimicrobial peptide activity and drug resistance. Curr Opin Chem Biol *52*, 85–
983 92. https://doi.org/10.1016/j.cbpa.2019.05.025.

984 83. Lan, C.C.E., Wu, C.S., Huang, S.M., Wu, I.H., and Chen, G.S. (2013). High-
985 Glucose environment enhanced oxidative stress and increased interleukin-8
986 secretion from keratinocytes. Diabetes *62*, 2530–2538.
987 https://doi.org/10.2337/db12-1714.

988 84. Ma, X.X., Liu, Q.K., Kuai, L., Ma, X., Luo, Y., Luo, Y., Song, J.K., Fei, X.Y., Jiang,
989 J.S., Wang, M.X., et al. (2023). The role of neutrophils in diabetic ulcers and
990 targeting therapeutic strategies. Int Immunopharmacol *124*.
991 https://doi.org/10.1016/j.intimp.2023.110861.

992 85. Mollinedo, F. (2019). Neutrophil Degranulation, Plasticity, and Cancer Metastasis.
993 Trends Immunol *40*, 228–242. https://doi.org/10.1016/j.it.2019.01.006.

994 86. Wang, L., Zhou, X., Yin, Y., Mai, Y., Wang, D., and Zhang, X. (2019).
995 Hyperglycemia induces neutrophil extracellular traps formation through an

NADPH oxidase-dependent pathway in diabetic retinopathy. Front Immunol *10*, 1–14. https://doi.org/10.3389/fimmu.2018.03076.

87. Ganesh, S., Don, K.R., and Priya.a, J. (2020). The role of matrix metalloproteinases in wound healing. International Journal of Pharmaceutical Research *12*, 702–707. https://doi.org/10.31838/ijpr/2020.SP2.087.

88. Gründling, A., and Schneewind, O. (2007). Synthesis of glycerol phosphate lipoteichoic acid in Staphylococcus aureus. Proc Natl Acad Sci U S A *104*, 8478–8483. https://doi.org/10.1073/pnas.0701821104.

89. Percy, M.G., and Gründling, A. (2014). Lipoteichoic acid synthesis and function in gram-positive bacteria. Annu Rev Microbiol *68*, 81–100. https://doi.org/10.1146/annurev-micro-091213-112949.

90. Dowey, R., Iqbal, A., Heller, S.R., Sabroe, I., and Prince, L.R. (2021). A Bittersweet Response to Infection in Diabetes; Targeting Neutrophils to Modify Inflammation and Improve Host Immunity. Front Immunol *12*, 1–21. https://doi.org/10.3389/fimmu.2021.678771.

91. Derré-Bobillot, A., Cortes-Perez, N.G., Yamamoto, Y., Kharrat, P., Couvé, E., Da Cunha, V., Decker, P., Boissier, M.C., Escartin, F., Cesselin, B., et al. (2013). Nuclease A (Gbs0661), an extracellular nuclease of Streptococcus agalactiae, attacks the neutrophil extracellular traps and is needed for full virulence. Mol Microbiol *89*, 518–531. https://doi.org/10.1111/mmi.12295.

92. Li, D., Pi, W., Sun, Z., Liu, X., and Jiang, J. (2022). Ferroptosis and its role in cardiomyopathy. Biomedicine and Pharmacotherapy *153*, 113279. https://doi.org/10.1016/j.biopha.2022.113279.

93. Goncheva, M.I., Chin, D., and Heinrichs, D.E. (2022). Nucleotide biosynthesis: the base of bacterial pathogenesis. Trends Microbiol *30*, 793–804. https://doi.org/10.1016/j.tim.2021.12.007.

94. Tan, C.A.Z., Chong, K.K.L., Yeong, D.Y.X., Ng, C.H.M., Ismail, M.H., Yap, Z.H., Khetrapal, V., Tay, V.S.Y., Drautz-Moses, D.I., Ali, Y., et al. (2024). Purine and carbohydrate availability drive Enterococcus faecalis fitness during wound and urinary tract infections. mBio *15*. https://doi.org/10.1128/mbio.02384-23.

95. Liu, G.Y., Doran, K.S., Lawrence, T., Turkson, N., Puliti, M., Tissi, L., and Nizet, V. (2004). Sword and shield: Linked group B streptococcal β-hemolysin/cytolysin and carotenoid pigment function to subvert host phagocyte defense. Proc Natl Acad Sci U S A *101*, 14491–14496. https://doi.org/10.1073/pnas.0406143101.

96. Spencer, B.L., Tak, U., Mendonça, J.C., Nagao, P.E., Niederweis, M., and Doran, K.S. (2021). A type VII secretion system in Group B Streptococcus mediates cytotoxicity and virulence. PLoS Pathog *17*, e1010121. https://doi.org/10.1371/journal.ppat.1010121.

1034 97. Mascher, T., Zähner, D., Merai, M., Balmelle, N., De Saizieu, A.B., and
1035 Hakenbeck, R. (2003). The Streptococcus pneumoniae cia regulon: CiaR target
1036 sites and transcription profile analysis. J Bacteriol *185*, 60–70.
1037 https://doi.org/10.1128/JB.185.1.60-70.2003.

1038 98. Alves, L.A., Harth-Chu, E.N., Palma, T.H., Stipp, R.N., Mariano, F.S., Höfling,
1039 J.F., Abranches, J., and Mattos-Graner, R.O. (2017). The two-component system
1040 VicRK regulates functions associated with Streptococcus mutans resistance to
1041 complement immunity. Mol Oral Microbiol *32*, 419–431.
1042 https://doi.org/10.1111/omi.12183.

1043 99. Madoff, L.C., Michel, J.L., and Kasper, D.L. (1991). A monoclonal antibody
1044 identifies a protective C-protein alpha-antigen epitope in Group B streptococci.
1045 Infect Immun *59*, 204–210. https://doi.org/10.1128/iai.59.1.204-210.1991.

1046 100. Casadaban, M.J., and Cohen, S.N. (1980). Analysis of gene control signals by
1047 DNA fusion and cloning in Escherichia coli. J Mol Biol *138*, 179–207.
1048 https://doi.org/10.1016/0022-2836(80)90283-1.

1049 101. Hooven, T.A., Bonakdar, M., Chamby, A.B., and Ratner, A.J. (2019). A
1050 Counterselectable Sucrose Sensitivity Marker Permits Efficient and Flexible
1051 Mutagenesis in Streptococcus agalactiae. Appl Environ Microbiol *85*, 1–13.
1052 https://doi.org/10.1128/AEM.03009-18.

1053 102. Mu, R., Kim, B.J., Paco, C., Del Rosario, Y.D., Courtney, H.S., and Doran, K.S.
1054 (2014). Identification of a group B streptococcal fibronectin binding protein, SfbA,
1055 that contributes to invasion of brain endothelium and development of meningitis.
1056 Infect Immun *82*, 2276–2286. https://doi.org/10.1128/IAI.01559-13.

1057 103. Chang, J.C., Jimenez, J.C., and Federle, M.J. (2015). Induction of a quorum
1058 sensing pathway by environmental signals enhances group A streptococcal
1059 resistance to lysozyme. Mol Microbiol *97*, 1097–1113.
1060 https://doi.org/10.1111/mmi.13088.

1061 104. Jeng, A., Sakota, V., Li, Z., Datta, V., Beall, B., and Nizet, V. (2003). Molecular
1062 genetic analysis of a group A Streptococcus operon encoding serum opacity
1063 factor and a novel fibronectin-binding protein, SfbX. J Bacteriol *185*, 1208–1217.
1064 https://doi.org/10.1128/JB.185.4.1208-1217.2003.

1065 105. DeJesus, M.A., Ambadipudi, C., Baker, R., Sassetti, C., and Ioerger, T.R. (2015).
1066 TRANSIT - A Software Tool for Himar1 TnSeq Analysis. PLoS Comput Biol *11*, 1–
1067 17. https://doi.org/10.1371/journal.pcbi.1004401.

1068 106. Li, H., and Durbin, R. (2009). Fast and accurate short read alignment with
1069 Burrows-Wheeler transform. Bioinformatics *25*, 1754–1760.
1070 https://doi.org/10.1093/bioinformatics/btp324.

1071 107. Mills, K.B., Maciag, J.J., Wang, C., Crawford, J.A., Enroth, T.J., Keim, K.C.,
1072 Dufrêne, Y.F., Robinson, D.A., Fey, P.D., Herr, A.B., et al. (2024).
1073 Staphylococcus aureus skin colonization is mediated by SasG lectin variation.
1074 Cell Rep *43*. https://doi.org/10.1016/j.celrep.2024.114022.

1075 108. Lang, J., Capasso, A., Jordan, K.R., French, J.D., Kar, A., Bagby, S.M., Barbee,
1076 J., Yacob, B.W., Head, L.S., Tompkins, K.D., et al. (2020). Development of an
1077 adrenocortical cancer humanized mouse model to characterize anti-PD1 effects
1078 on tumor microenvironment. Journal of Clinical Endocrinology and Metabolism
1079 *105*, 26–42. https://doi.org/10.1210/clinem/dgz014.

1080 109. Miller, R.J., Crosby, H.A., Schilcher, K., Wang, Y., Ortines, R. V., Mazhar, M.,
1081 Dikeman, D.A., Pinsker, B.L., Brown, I.D., Joyce, D.P., et al. (2019). Development
1082 of a Staphylococcus aureus reporter strain with click beetle red luciferase for
1083 enhanced in vivo imaging of experimental bacteremia and mixed infections. Sci
1084 Rep *9*, 1–19. https://doi.org/10.1038/s41598-019-52982-0.

1085 110. Bhattacharya, M., Berends, E.T.M., Chan, R., Schwab, E., Roy, S., Sen, C.K.,
1086 Torres, V.J., and Wozniak, D.J. (2018). Staphylococcus aureus biofilms release
1087 leukocidins to elicit extracellular trap formation and evade neutrophil-mediated
1088 killing. Proc Natl Acad Sci U S A *115*, 7416–7421.
1089 https://doi.org/10.1073/pnas.1721949115.

1090 111. Bhattacharya, M., Berends, E.T.M., Zheng, X., Hill, P.J., Chan, R., Torres, V.J.,
1091 and Wozniak, D.J. (2020). Leukocidins and the Nuclease Nuc Prevent Neutrophil-
1092 Mediated Killing of Staphylococcus aureus Biofilms. Infect Immun *88*, 1–16.
1093 https://doi.org/10.1128/IAI.00372-20.

1094 112. Kao, P.H.-N., Ch'ng, J.-H., Chong, K.K.L., Stocks, C.J., Wong, S.L., and Kline,
1095 K.A. (2023). Enterococcus faecalis suppresses Staphylococcus aureus-induced
1096 NETosis and promotes bacterial survival in polymicrobial infections. FEMS
1097 microbes *4*, xtad019. https://doi.org/10.1093/femsmc/xtad019.

1098 113. Freeman, C.D., Hansen, T., Urbauer, R., Wilkinson, B.J., Singh, V.K., and Hines,
1099 K.M. (2024). Defective pgsA contributes to increased membrane fluidity and cell
1100 wall thickening in Staphylococcus aureus with high-level daptomycin resistance.
1101 mSphere *9*, e0011524. https://doi.org/10.1128/msphere.00115-24.

1102 114. Tiwari, K.B., Sen, S., Gatto, C., and Wilkinson, B.J. (2021). Fluorescence
1103 Polarization (FP) Assay for Measuring Staphylococcus aureus Membrane Fluidity.
1104 In Staphylococcus aureus: Methods and Protocols, K. C. Rice, ed. (Springer US),
1105 pp. 55–68. https://doi.org/10.1007/978-1-0716-1550-8_8.

1106

1107

1108 **Materials and Methods**

1109 **Bacterial strains**

1110 All strains used in the study are listed in STAR Methods. GBS strains were grown
1111 statically at 37°C in Todd-Hewitt broth (THB). *Escherichia coli* strains were grown in
1112 lysogeny broth at 37°C or 30˚C with rotation at 225 rpm. Erythromycin and spectinomycin
1113 (Sigma-Aldrich) were supplemented to media at 300 and 100 µg/mL for *E. coli* or 5 and
1114 100 µg/mL for GBS strains, respectively.

1115 **Animals**

1116 For murine diabetic wound 8 to 12-week-old male mice from the C57Bl/6J or *Lepr*$^{db}$
1117 background were used. Animal experiments were approved by the Institutional Animal
1118 Care and Use Committee at University of Colorado Anschutz Medical Campus protocol
1119 no. 00987 and were performed using accepted veterinary standards. The University of
1120 Colorado Anschutz Medical Campus is AAALAC accredited, and its facilities meet and
1121 adhere to the standards in the Guide for the Care and Use of Laboratory Animals.

1122

1123 **Routine molecular biology techniques**

1124 All PCR reactions utilized Phusion polymerase (New England Biolabs). PCR products
1125 and restriction digest products were purified using Qiagen PCR purification kit (Qiagen)
1126 per manufacturer protocols. See Table S3 for primers. Plasmids were extracted using
1127 Qiagen plasmid mini and maxiprep kits (Qiagen) per manufacturer protocols. Restriction
1128 enzyme digests utilized XhoI, PstI, BamHI, and SacII (New England Biolabs) for at least
1129 3 h at 37°C. Ligations utilized T4 DNA ligase (New England Biolabs) at 16°C overnight.
1130 All plasmid constructs were sequence confirmed by Nanopore amplicon sequencing
1131 (Quintara Biosciences).

1132

1133 **Construction of *dltA* and *cpsD* knockout plasmid**

1134 Construction of the *dltA* clean deletion knockout plasmid was performed as previously
1135 described [43,44]. Briefly, approximately 1.5 kb upstream and downstream of the CJB111
1136 *dltA* (ID870_00720), or *cpsD* (ID870_03500) and the spectinomycin cassette from
1137 plasmid JC303 [103] was amplified using PCR. Plasmid, pMBSacB [101], and the PCR
1138 products were digested using appropriate restriction enzymes and ligated overnight and
1139 transformed into chemically competent *E. coli* MC1061 as described [43]. Cultures were
1140 pelleted using an Eppendorf 5810R centrifuge at 3900 x g for 10 min at room temperature.
1141 Plasmid was extracted as described above and sequence verified via Nanopore whole
1142 plasmid sequencing (Quintara Biosciences).

1143

1144 **Deletion and complementation of CJB111 *dltA* and *cpsD***

1145 GBS electrocompetent cells were generated as described and double crossover
1146 homologous recombination knockout strategy was performed as described previously

1147 [43,44]. For *dltA,* after the second cross-over, GBS was incubated in THB + 0.75 M sucrose
1148 and 100 µg/mL spectinomycin at 37°C before plating on THB agar supplemented with
1149 100 µg/mL spectinomycin, whereas *cpsD* is a clean deletiona dn no spectinomycin
1150 cassette. Colonies were PCR screened for loss of gene using primers outside of the
1151 recombination arms and grown in THB at 37˚C and stocked. Sequence confirmation of
1152 the mutants was done via Nanopore sequencing (Quintara Biosciences). The pJDltA
1153 complementation plasmid was constructed as previously described [43,44]. CJB111 *dltA*
1154 gene was amplified, restriction digested and ligated overnight into pDCErm [104] plasmid
1155 backbone. Ligations were transformed into *E. coli* for maintenance. Complement
1156 plasmids sequence confirmed as above and were electroporated into GBS
1157 electrocompetent cells prepared as described above.

1158

1159 **Murine model of diabetic wound infection**

1160 8 to 12-week-old male mice from the C57Bl/6J or *Lepr$^{db}$* background were used
1161 throughout the study. Two weeks prior to infection mice were given low dose injections of
1162 Streptozotocin (50mg/kg) (CAS-No: 18883-66-4) dissolved immediately before injection
1163 in 100 µL of 50 mM sodium citrate buffer (pH 4.5) for 5 consecutive days, followed by a
1164 glucose chaser (250 µL) to prevent hypoglycemia [77]. Mice then sat for a minimum of one
1165 week for blood sugar to normalize before infection. Mice were infected as previously
1166 described [77]. Briefly, the day before infection mice were anesthetized via isoflurane
1167 inhalation, shaved and treated with Nair on the back. Tail snips were performed and blood
1168 sugar measured via glucometer to ensure all mice had blood glucose levels >200 mg/dl.
1169 The following day, mice were weighed and anesthetized via isoflurane inhalation and
1170 injected with lidocaine intra-dermally. Mice were wounded with a 6 mm biopsy punch and
1171 inoculated with 1 x $10^7$ CFU GBS or a PBS control unless otherwise indicated. Wounds
1172 were wrapped with the surgical adhesive Tegaderm for 5 h before adhesive removal and
1173 monitoring of animals. After 48 h of infection, mice were sacrificed and wound as well as
1174 kidneys were harvested for further analysis. Tissues were placed into 500 µl of sterile
1175 PBS in 2.0-ml conical tubes (Thermo Fisher Scientific) along with 1.0-mm-diameter
1176 zirconia/silica beads (BioSpec catalog no. 1107911) and homogenized by bead beating
1177 two times for 60 s in a BioSpec mini bead beater. Tissue homogenates were plated on
1178 GBS CHROMagar [SB282(B)], which allows only for the growth of GBS (in pink) and
1179 Enterococcus spp. (in blue). These experiments were approved by the committee on the
1180 use and care of animals at the University of Colorado–Anschutz Medical Campus protocol
1181 no. 00987. For neutrophil depletion experiments, mice were injected with 200 µg of either
1182 anti-Ly6G (BioXCell, clone 18A, catalog BE0075-1) or anti-IgG2a isotype control antibody
1183 (BioXCell, clone 2A3, catalog BE0089) diluted in buffered reagent diluent (BioXCell,
1184 catalog IP0070) the day before infection.

1185

1186 **Diabetic wound transposon library infection**

1187 Triplicate cultures of the pooled CJB111 pKrmit transposon library [49] were grown
1188 overnight at 37˚C in THB with kanamycin at 300 µg/mL and grown to exponential phase
1189 without kanamycin before libraries were normalized to ~1.5 x $10^7$ CFU/10 µL and *Lepr$^{db}$*

1190 mice were infected as described above. Input library and wound homogenate was plated
1191 in duplicated on CHROMagar Strep B with 300 µg/mL kanamycin and incubated overnight
1192 at 37˚C to collect recovered transposon mutants. Bacterial growth from spread plates
1193 were collected and 4 mice per library pooled together before genomic DNA was extracted
1194 using ZymoBiomics DNA miniprep Kit (Zymo Research).

1195

1196 **Transposon library sequencing**

1197 Libraries were prepared and sequenced at the University of Minnesota Genomics Center
1198 (UMGC) according to https://www.protocols.io/view/transposon-insertion-sequencing-tn-
1199 seq-library-pre-rm7vzn6d5vx1/v1. Briefly, genomic DNA was enzymatically fragmented,
1200 and adapters added using the NEB Ultra II FS kit (New England Biolabs), and ~50 ng of
1201 fragmented adapted gDNA was used as a template for enrichment by PCR (16 cycles)
1202 for the transposon insertions using mariner-specific
1203 (TCGTCGGCAGCGTCAGATGTGTATAAGAGACAGCCGGGGACTTATCATCCAACC)
1204 and Illumina P7 primers. The enriched PCR products were diluted to 1ng/ul and 10 ul was
1205 used as a template for an indexing PCR (9 cycles) using Nextera_R1 (iP5) and
1206 Nextera_R2 (iP7) primers. Sequencing was performed using 150- base paired-end format
1207 on an Illumina NovaSeq 6000 system to generate ~40 million reads per library.

1208

1209 **Tn-seq bioinformatics analyses**

1210 Bioinformatic analyses were performed as previously described [50] Reads were trimmed
1211 using Cutadapt (v 4.2) with the following parameters: sequence length with a minimum of
1212 12 bases, removal of flanking "N" bases, reads were trimmed of 3' "G" bases, and reads
1213 were trimmed with the reverse complemented mariner transposon sequence
1214 (ACTTATCAGCCAACCTGTTA). TRANSIT (v 3.2.7) [105] was used to align trimmed reads
1215 to the CJB111 genome (CP063198) for analysis of transposon insertion sites. The Transit
1216 PreProcessor processed reads using default parameters with the Sassetti protocol, no
1217 primer sequence, and mapped them to the genome using Burrows-Wheeler Alignment
1218 (BWA) [106]. Insertion sites were normalized using the total trimmed reads (TTR) in
1219 TRANSIT and analyzed using the site-restricted resampling to compare the insertion
1220 counts recovered in wound vs the input library. Resampling was performed using default
1221 parameters, with the addition of ignoring TA sites within 5% of the 5' and 3' end of the
1222 gene. All sequencing reads have been deposited into NCBI SRA under BioProject
1223 accession PRJNA1232139.

1224

1225 **N/TERT adherence, invasion and intracellular survival assays**

1226 Human immortalized N/TERT-2G keratinocyte cells [74,107] were seeded at 1 x $10^5$ cells in
1227 keratinocyte serum-free medium (KSFM, Gibco) supplemented with 0.3 mM calcium
1228 chloride (PromoCell) in a 24-well tissue culture treated plate and incubated at 5% $CO_2$
1229 and 37°C. Assays to determine the total number of bacteria adhered to host cells or
1230 intracellular bacteria were performed using GBS empty vector and complement strain as

1231 described previously [43,44]. Briefly, exponential phase bacteria were normalized to 1 x $10^8$
1232 CFU/mL in PBS and 1 x $10^5$ CFU per well at multiplicity of infection (MOI) of 1. The total
1233 cell associated GBS were recovered after 30 min incubation. Cells were washed four
1234 times with 1X PBS (Sigma) and detached by addition of 100 µL of 0.25% trypsin-EDTA
1235 solution (Gibco) and incubation for 5 min at 37˚C before lysing the eukaryotic cells with
1236 the addition of 400 µL of 0.025% Triton X-100 (Sigma) and vigorous pipetting. The lysates
1237 were serially diluted and plated on THB agar and incubated overnight to determine CFU.
1238 Bacterial invasion assays were performed as described above except infection plates
1239 were incubated for 2 h before incubation with 100 µg gentamicin (Sigma) and 5 µg
1240 penicillin (Sigma) supplemented media for an additional 2 h to kill all extracellular bacteria,
1241 prior to being trypsinized, lysed, and plated as described. Experiments were performed
1242 in biological triplicate with three technical replicates per experiment.

1243

1244 **Dissociation of wound tissue and blood for flow cytometry**

1245 Single cell suspension preparation was performed using methods previously described
1246 by our group [47]. In brief, following euthanasia, mice were perfused with PBS+heparin and
1247 wounds were excised, minced with a razor blade, and suspended in 2.4 mL RPMI 1640
1248 medium (Corning). Digestion enzymes were obtained from Miltenyi Biotec Multi Tissue
1249 Dissociation Kit 1 and resuspended according to manufacturer instructions. 100 µL
1250 Enzyme D, 50 µL Enzyme R, 12.5 µL Enzyme A were added to each tissue sample in
1251 RPMI. Tissues were mechanically dissociated using gentleMACS™ C Tubes (Miltenyi
1252 Biotec; protocol Multi H) for 30 sec, incubated on a rocking shaker at 37°C for 30 min,
1253 followed by an additional 30 sec of mechanical dissociation and 30 min incubation at 37˚C
1254 while rocking. The digestion mixture was strained through a 70 µm filter, and the single
1255 cells were washed with RPMI and spun down at 300 x g for 5 min. The cell pellet was
1256 resuspended in Ammonium-Chloride-Potassium red blood cell lysis buffer (150 mM
1257 NH4Cl, 10 mM KHCO3, 0.1 mM Na2EDTA) for 1 min at room temperature and diluted in
1258 RPMI. Following centrifugation, the cell pellet was resuspended in MACS staining buffer
1259 (1X PBS, 2 mM EDTA, 0.5% BSA) to generate single cell suspensions. Blood was
1260 obtained from right ventricle cardiac puncture. Approximately 200 µL were taken from
1261 each animal and mixed a small amount of heparin suspended in PBS. Ammonium-
1262 Chloride-Potassium red blood cell lysis buffer was added to blood samples to a final
1263 volume of 1 mL, and incubated for 3 min. Samples were then spun down at 300 x g for 5
1264 min and the resulting pellet was washed again in red blood cell lysis buffer with a repeat
1265 spin. The cell pellet was resuspended in MACS staining buffer to generate single cell
1266 suspensions as noted above.

1267

1268 **Antibody staining of single cell suspensions for flow cytometry analysis**

1269 Antibody staining methods and panels were performed as previously described [47]. Fixable
1270 Viability Dye eFluor™ 506 (ThermoFisher; 1:800 dilution) in PBS was added to single cell
1271 suspensions and allowed to incubate for 15 min at room temperature. Conjugated
1272 antibodies listed in Table S4 were then added to wound and blood single cell suspensions
1273 along with anti-mouse CD16/32 (ThermoFisher, Fc block, clone 93) for 30 min at room

temperature. To analyze human neutrophils, antibodies against surface markers listed in Table S4 were added with human FcR Blocking Reagent (Miltenyi Biotec). Stained neutrophils were then washed and fixed using Foxp3/Transcription Factor Staining Buffer Set (eBioscience) according to the manufacturer's protocol. Cells were analyzed on the LSRFortessa (BD Biosciences) flow cytometer. Data were analyzed with BD FlowJo software version 10.10.0. Single-stained beads (Versacomp Antibody Capture Bead Kit; Beckman Coulter) were used as compensation controls. A detailed gating strategy is included in Figure S1 for wound and blood and Figure S6 for neutrophil degranulation.

**Multispectral Immunohistochemistry and Image Analysis**

Diabetic mice were wounded and infected with either WT CJB111 expressing GFP or mock infected with PBS as described above. After 48h of infection, animals were sacrificed and wounds excised and sent to the Human Immune Monitoring Shared Resource (HIMSR) at the University of Colorado Anschutz Medical Center. Multispectral immunohistochemistry (mIHC) analyses were performed using Vectra Automated Quantitative Pathology Systems (Akoya Biosciences) as described previously [108]. Tissues were formalin-fixed, paraffin embedded and sectioned onto slides. Whole tissues were analyzed with the following antibodies; MsCD11b (Novus, NB110-89474), Msly6G (CST, 87048S), HuCitH3 (abcam, ab5103), MsGFP/YFP (CST, 2956S), msCD11c (CST, 97585S), MsCD45 (CST, 70257S), MsEpCAM (CST, 93790S), MsF480 (CST, 30325S), and DAPI. All slides were deidentified and imaged by the Anschutz Medical Campus Human Immune Monitoring Shared Resource (HIMSR) core (RRID:SCR_021985) on Akoya Biosciences PhenoImager HT scanner. Regions of interest (ROI) were selected, and multispectral images were collected with the 20× objective. A training set of nine representative images was used to train the analyses algorithms for tissue and cell segmentation and phenotyping using in Form software (Akoya Biosciences). Representative autofluorescence was measured on an unstained control slide and subtracted from study slides.

**Primary human neutrophil killing**

Primary human neutrophils were isolated from healthy human donors (female $n = 2$, male $n = 2$) per the COMIRB protocol number 17-1926 as previously described [109–111]. Neutrophils were resuspended in RPMI (Gibco, no phenol red) with 22 mM glucose to mimic diabetes [46]. Mid-exponential phase GBS were normalized to 1 x $10^8$ CFU/mL in Hanks' Balanced Salt Solution (HBSS, Gibco), and 1mL GBS was opsonized in 10% pooled human serum (Complement Tech) at 37˚C with rotation for 30 min. Opsonized GBS were washed once with HBSS before being resuspended in 1 mL of 4 x $10^6$ neutrophils (MOI of 25) and split into two Eppendorf tubes containing 500 µL each. One tube was incubated at 37˚C, with rotation, for 1 h and the second tube used for time 0 h counts. At each time point, 500 µL of 0.05% Saponin (Sigma) was added to the tube and vortex vigorously to lyse neutrophils. 20 µL was removed in duplicate and serial diluted and 50 µL was spread plate on THA containing plates and incubate at 37˚C overnight for

1316 CFU enumeration. Percent survival was calculated as the ratio of CFU at 1 h verses 0 h
1317 and normalized to the no neutrophil control (RPMI only tubes) set to 100%.

1318

1319 **HL60 opsonophagocytic killing**

1320 HL60 opsonophagocytic killing assays were performed as previously described [43]. Briefly,
1321 HL60 cells purchased from ATCC (ATCC CCL-240) were differentiated with 1.25%
1322 DMSO (Sigma) in RPMI for 4 days. Differentiated HL60 cells were harvested and checked
1323 for > 65% viability before starting the assay in accordance with a well-characterized
1324 protocol. In a 96 well plate (Corning), 50 µL containing ~1 x$10^3$ CFU of mid-exponential
1325 phase GBS, normalized in HBC buffer (1X HBSS, 0.5% BSA, and 2.2 mM $CaCl_2$, pH 7.2)
1326 was added. 50 µL of either 20% normal human serum (Complement Tech) or 20% heat-
1327 killed human serum (60˚C for >30 min) in HBC buffer were added to each well and
1328 incubated at 37˚C, with shaking, for 15 min. 100 µL of HL60 cells (~5 x$10^5$) were added
1329 to each well and incubated at 37˚C with shaking, MOI ~0.001, as previously described.
1330 Over a 3h time course, 10 µL's were removed and indicated times, serial diluted and
1331 plated on THB agar for enumeration. Assays were performed in biological triplicate with
1332 technical duplicates per replicate. Percent survival was calculated as the ratio of CFU in
1333 normal serum versus CFU in heat-killed serum, and no HL60 control wells were set to
1334 100%.

1335

1336 **HL60 opsonophagocytic uptake measured by imagestream flow cytometry**

1337 GBS were opsonized as described above and HL60-neutrophil like cells were infected at
1338 an MOI of 8 - 10 for 15 minutes at 37˚C with rotation. Following incubation tubes were
1339 transferred to ice and washed in MACS staining buffer described above. To stain the host
1340 cell surface, HL-60s were incubated with anti-human CD11b (cat no. 301309, clone
1341 [ICRF44]) and anti-human CD45 (cat no. 304011, clone [HI30]) both conjugated to APC
1342 along with human FcR Blocking Reagent (Miltenyi Biotec). Cells were fixed using
1343 Foxp3/Transcription Factor Staining Buffer Set (eBioscience) according to the
1344 manufacturer's protocol. Samples were run on the Imagestream Mark II cytometer (Cytek
1345 Bioscieces) using the 60x objective. Samples were then analyzed with the IDEAS v6.4
1346 software (Cytek Biosciences). For analysis masks were made using the object and
1347 adaptive erode functions for generating cell, inside the cell and the membrane masks.
1348 The samples were first gated on area vs aspect ratio for single cells, and only in focused
1349 cells were included. Focused cells were then gated on $CD45^+CD11b^+$ expression using
1350 the membrane mask and intensity per area feature. GBS bacteria on the membrane,
1351 inside the cell or both were numerate with the threshold function mask and the spot count
1352 feature. The assay was performed in biological quadruplicate.

1353

1354 **Primary human neutrophil degranulation**

1355 To measure degranulation in primary human neutrophils, neutrophils were isolated as
1356 described above and infected with opsonized GBS at an MOI of 25 in 22 mM glucose as

1357 described above for 30 min at 37˚C in a 96 well plate. Antibody staining and flow
1358 cytometry analysis is described above using known markers of degranulation [85,112].

1359

1360 **Cationic antimicrobial peptide killing**

1361 mCRAMP killing assays were performed with concentrations as previously described [43].
1362 A total of 2-4 x $10^5$ CFU of mid-exponential phase cultures were exposed to 20 µM
1363 mCRAMP (AnaSpec) in THB for 30 min at 37˚C. Dilutions were plated for CFU
1364 enumeration.

1365

1366 **Reactive oxygen species susceptibility and 8-OHdG ELISA**

1367 Overnight cultures were normalized to 1 x $10^8$ CFU/mL and 2 mL of bacteria were
1368 exposed to 0.08% hypochlorite (Clorox) or 100 µg of hydrogen peroxide (Millipore,
1369 386790) for 1 h at 37˚C before 10 µL was removed for serial dilution and plating for CFU
1370 on THA plates. The rest of the bacteria exposed to hydrogen peroxide were pelleted and
1371 stored at -20 ˚C for 8-OHdG Quantification via OxiSelect Oxidative DNA Damage ELISA
1372 Kit (Cell Biolabs, STA-320) per manufacturer protocol. Biological triplicate was performed.

1373

1374 **Transmission electron microscopy**

1375 TEM was performed at the electron microscopy core facility at the University of Colorado
1376 Anschutz Medical Campus. Approximately 8 mL of mid-exponential ($OD_{600nm}$ 0.5 – 0.6)
1377 growing bacteria were pelleted and cells were fixed with 2% paraformaldehyde and
1378 2% glutaraldehyde in 0.1M sodium cacodylate buffer and embedded in 3% agarose.
1379 Samples were trimmed into small bocks and rinsed three rinses in 0.1 M sodium
1380 cacodylate buffer, they were post-fixed in 2% osmium tetroxide and 0.8 % $K_3[Fe(CN_6)]$ in
1381 0.1 M sodium cacodylate buffer for 1 h at room temperature. Cells were rinsed with water
1382 and en bloc stained with 2% aqueous uranyl acetate for 1 h. They were dehydrated with
1383 increasing concentration of ethanol, infiltrated with SPURR resin and polymerized in a
1384 60˚C oven overnight. Blocks were sectioned with a diamond knife (Diatome) on a UC7
1385 ultramicrotome (Leica) and collected onto copper grids, post stained with 2% aqueous
1386 uranyl acetate and lead citrate. Images were acquired on a Tecnai T12 transmission
1387 electron microscope (ThermoFisher) equipped with a $LaB_6$ source at 80 kV using an
1388 NS15 (15 Mpix) camera (AMT).

1389

1390 **GBS capsule flow cytometry**

1391 Flow cytometry for capsule expression was performed using CJB111 WT, CJB111Δ*iagB*,
1392 CJB111Δ*iagA*, CJB111Δ*mprF,* CJB111Δ*dltA,* and CJB111Δ*cpsD* empty vector strains,
1393 the respective complement strains, pJIagB, pJIagA, pJMprF, and pJDltA, and GBS A909
1394 (Ia Capsule). Overnight cultures were washed in HBC buffer (Hanks' balanced salt
1395 solution [HBSS]-bovine serum albumin-calcium buffer; 1× HBSS without magnesium or
1396 calcium, 0.5% bovine serum albumin, 2.2 mM $CaCl_2$) and incubated with adsorbed anti-

Group B serotype V antisera (SSI Diagnostica Group, cat. no 22461) at a 1:5000 dilution. Bacteria were washed via centrifugation and labeled with a goat anti-rabbit Ig conjugated to AF647 (SouthernBiotech, cat. no 4010-31) at a 1:5000 dilution. Bacteria were fixed in 5% formalin and analyzed on a BD LSRFortessa (BD Biosciences) using the BD FacsDiva software (v9). Data were anlyzed with BD FlowJo software v 10.10.

### Anisotropy

The small molecule probe 1,6-diphenyl-1,3,5-hexatriene (Sigma; DPH) was used to evaluate membrane fluidity as previously described [113,114]. Briefly, pellets from overnight cultures were washed with phosphate buffered saline (PBS) twice and resuspended in fresh PBS to ~ 1 x $10^8$ CFU/mL in 3 mL of PBS and incubated with 5 μM of DPH for 15 min at 37°C and 200 rpm and samples were kept at 37˚C using a water bath until analyzed. Anisotropy measurements were taken on a Jobin Yvon FluoroMax-3 spectrofluorometer with polarizers in the L geometry at the Biophysics Shared Research Facility at the University of Colorado Anschutz Medical Campus. DPH was excited at 360 nm and the fluorescence intensity was monitored at 430 nm. Samples were maintained at 37°C using the temperature-controlled sample compartment of the spectrofluorometer. Measurements were performed on biological quadruplicate. The anisotropy of DPH was calculated from the differences in the fluorescence intensity detected with the polarizers in the vertical and horizontal orientations and data is reported in arbitrary units (AU). Biological quadruplicate was performed.

## QUANTIFICATION AND STATISTICAL ANALYSIS

Statistical details of each experiment including statistical tests, number of samples, and significance threshold can be found in the figure legends. All statistical analysis was performed using GraphPad Prism software version 10 (San Diego, California) unless otherwise indicated, and statistical significance was accepted at p-values of $< 0.05$.